UNIVERSITY OF
CALIFORNIA

Radiation Laboratory

BERKELEY, CALIFORNIA

DISCLAIMER

UCRL-2307
Unclassified - Physics
Distribution

UNIVERSITY OF CALIFORNIA

Radiation Laboratory

Contract No. W-7405-eng-48

ELASTIC AND INELASTIC SCATTERING OF 90-MEV NEUTRONS BY DEUTERONS

Byron L. Youtz

(Thesis)

August 13, 1953

Berkeley, California

UNITED STATES ATOMIC ENERGY COMMISSION

UCRL-2307

ELASTIC AND INELASTIC SCATTERING OF 90-MEV NEUTRONS BY DEUTERONS (thesis)

By
Byron L. Youtz

August 13, 1953

Radiation Laboratory
University of California, Berkeley

Technical Information Service, Oak Ridge, Tennessee

TABLE OF CONTENTS

PHYSICS

PRINTED IN USA
PRICE 55 CENTS
Available from the
Office of Technical Services
Department of Commerce
Washington 25, D. C.

Work performed under
Contract No. W-7405-eng-48.

AEC, Oak Ridge, Tenn.-W36669

ELASTIC AND INELASTIC SCATTERING OF 90-MEV NEUTRONS BY DEUTERONS

Byron L. Youtz

Radiation Laboratory, Department of Physics,
University of California, Berkeley, California

August 13, 1953

ABSTRACT

The differential cross sections were measured for the elastic scattering and for the n-p type of inelastic scattering of 90-Mev neutrons by deuterons. The neutrons, produced in the stripping of 190-Mev deuterons by a beryllium target in the Berkeley 184-inch synchrocyclotron, have an energy distribution centered at 90 Mev with a spread of 30 Mev full width at the half-maximum. Normalization of the cross sections was made by comparison to the n-p scattering cross sections of Hadley et al. The angular range between five degrees and forty degrees in the laboratory system was covered for both the elastic and inelastic reactions with $2\text{-}1/2^{\circ}$ angular resolution.

The experimental data are compared to the theory of Chew, which uses the impulse approximation with central forces only, and to the theory of Horie, Tamura, and Yoshida, which is based on the Born approximation but includes both central and tensor forces. Furthermore, the data for elastic scattering are shown to be in satisfactory agreement, over the angular range covered here, with the results of Stern for 190-Mev deuteron-proton scattering, thus lending further support to the idea of charge independence of nuclear forces at moderately high energies.

ELASTIC AND INELASTIC SCATTERING OF 90-MEV NEUTRONS BY DEUTERONS

Byron L. Youtz

Radiation Laboratory, Department of Physics,
University of California, Berkeley, California

August 13, 1953

I INTRODUCTION

The nature of the nuclear force continues to be one of the most basic problems of nuclear physics. A considerable body of precise experimental data has been accumulated in the region of low interaction energy between nuclear particles, and a theory requiring little specific detail of the nuclear force is now able to account for the results rather well.[1] One of the most interesting results of this low-energy work is the apparent charge independence of nuclear forces. From the data on stability and binding energies of the light nuclei, one concludes that neutron-neutron and proton-proton forces are equal except for Coulomb effects. Also, it has been shown by Schwinger[1] that the low-energy neutron-proton and proton-proton scattering experiments can be explained by assuming the nuclear forces to be equal and including both the electrostatic and the electromagnetic interactions to account for the observed differences.

As experiments with much higher interaction energies became feasible, rather startling results began to appear. The wave lengths of incident particles were then small enough to probe the detail of the nuclear force field. Exchange forces, postulated in connection with the low-energy data to explain saturation of the nuclear force, now became directly measurable from the shape of the neutron-proton differential scattering cross section.[2,3] Soon the high-energy proton-proton scattering data were available[4] and were found to bear very little resemblance to the curve predicted from the best n-p potential. The best fit to the p-p scattering data was obtained by adding a strong,

odd-wave tensor force to the above potential.[5] This potential still allowed a good fit to the n-p scattering data so that the charge-independence hypothesis could still be retained. Introduction of a hard core by Jastrow[6] to regain the necessary saturation property and modifications introduced by Levy[7] have greatly improved the status of the theory without seriously affecting the fit of the scattering curves to the experimental data. It is fairly evident that this course of evolution for the nuclear force is in no way unique; for example, Case and Pais[8] use a velocity-dependent force by including a spin-orbit coupling term, but even in this type of interaction it is felt that charge independence can be retained.

Since the present experimental data leave open the question of charge independence, and because of the fundamental nature of the problem, it is of utmost importance to collect as much additional experimental evidence as possible to test this point. Several meson production experiments are in progress, both at Chicago[9] and at Berkeley, in search of meson evidence for charge independence. Also, at Berkeley, a group of scattering experiments has been in progress for some time to collect data on this subject. Dr. Martin Stern[10] and Dr. Arnold Bloom[11] have measured the elastic and inelastic scattering of 190-Mev deuterons by protons; the experiment reported herein is an attempt to improve existing data[12] on the elastic and inelastic scattering of 90-Mev neutrons by deuterons; Dr. David Clark[13] has measured the elastic scattering of 340-Mev protons by deuterons; and the scattering of 300-Mev neutrons by deuterons may be undertaken in the near future.

The data of Stern and Bloom are of particular interest in relation to this experiment, since the center-of-mass interaction energies for the two cases are very nearly equal. Comparison between these experiments thus affords a rather direct test of the charge-independence hypothesis at moderately high energy.

II KINEMATICS

Elastic Scattering

The elastic scattering of neutrons by deuterons is a two-body reaction for which definite angular and energy relations can be derived from the principles of relativistic mechanics. We wish to find here the equations relating

1. deuteron energy and deuteron emission angle for the laboratory system;
2. center-of-mass scattering angle and laboratory-system emission angle for the deuteron;
3. center-of-mass and laboratory-system solid angles in terms of parameters of the laboratory system.

Neutron-proton scattering, used in normalizing the present data, is an almost identical kinematic problem and is also discussed here.

As indicated in Fig. 1, let the quantities for neutron-deuteron scattering be defined in the following way: Φ and $\textcircled{H}$ are the respective angles of emission of the deuteron and neutron in the laboratory system, θ is the center-of-mass scattering angle for either the neutron or the deuteron. These definitions follow the precedent of Stern[10] with respect to incident and target particles. Let $R = M_o c^2$ and take $P = pc$ for the relativistic momentum and E for the total relativistic energy of a particle in the laboratory system. Let β_c be the ratio of the velocity of the center of mass to the velocity of light and define $\gamma_c = (1 - \beta_c^2)^{-1/2}$

The following relations then exist:

$$\beta_c = \frac{\text{Total relativistic momentum, lab. system}}{\text{Total relativistic energy, lab. system}} = \frac{P_{on}}{E_{on} + R_d}$$

$$\gamma_c = \frac{E_{on} + R_d}{\sqrt{(E_{on} + R_d)^2 - P_{on}^2}} \qquad \tan \frac{\theta}{2} = \frac{1}{\gamma_c} \cot \Phi$$

$$T_d = 2R_d\beta_c^2 \frac{\gamma_c^2 \cos^2\Phi}{\gamma_c^2 \sin^2\Phi + \cos^2\Phi}$$

$$\frac{d\Omega_{lab}}{d\Omega_{cm}} = \frac{d\cos\Phi}{d\cos\theta} = \frac{\gamma_c^2}{4\cos\Phi}(1 - \beta_c^2\cos^2\Phi)^2$$

These equations are also valid for neutron-proton scattering if R_p is substituted for R_d throughout.

At 90 Mev incident-neutron energy, β_c is only 0.145, so the relativistic effects are just beginning to be noticed. Hence, the nonrelativistic equations are useful as a guide in planning the experiment. In this approximation, β_c approaches zero, γ_c goes to one, and $R_d\beta_c^2$ becomes $M_d v_c^2$. One then obtains, for n-D scattering,

$$\tan\frac{\theta}{2} = \cot\Phi \quad \text{or} \quad \theta = \pi - 2\Phi;$$

$$\frac{d\Omega_{lab}}{d\Omega_{cm}} = \frac{1}{4\cos\Phi}; \quad \text{and} \quad T_d = \frac{8}{9}T_n\cos^2\Phi.$$

For n-p scattering, the angle and solid-angle relations are the same and the equation for the energy of the emitted proton now has the familiar form:

$$T_p = T_n\cos^2\Phi$$

Table I gives values for θ, $\frac{d\Omega_{lab}}{d\Omega_{cm}}$, T_d, and T_p, for 90 Mev incident neutron energy and for various values of Φ. Variations in θ and $d\Omega_{lab}/d\Omega_{cm}$ due to the spread in energy of the incident neutrons amounts to less than one half percent from the values given here. Figure 2 shows the variation of the kinetic energy of the deuteron with its angle of emission, for various incident-neutron energies.

Table I

ϕ	θ		$d\Omega_{lab}/d\Omega_{cm}$		T_d(Mev)		T_p(Mev)	
	rel.	non-rel.	rel.	non-rel.	rel.	non-rel.	rel.	non-rel.
0°	180°	180°	0.2448	0.2500	80.67	80.0	89.96	90.0
15	149°42'	150	0.2541	0.2590	75.16	74.7	83.66	84.0
30	119°28'	120	0.2856	0.2885	60.17	60.0	66.67	67.5
45	89°24'	90	0.3536	0.3539	39.91	40.0	43.93	45.0
60	59°28'	60	0.5053	0.5000	19.94	20.0	21.71	22.5
75	29°42'	30	0.9840	0.9670	5.15	5.4	5.77	6.0
90	0° 0'	0	∞	∞	0.00	0.0	0.00	0.0

Inelastic Scattering

The inelastic scattering of neutrons by deuterons involves three-body kinematics, so that one cannot hope to find exact equations relating the variables of the reaction. However, the interaction between the particles within the deuteron is small enough so that they can be treated as free particles in obtaining an approximate notion of the collision kinematics. That is, a 90-Mev incident neutron has a de Broglie wave length of 0.95×10^{-13} cm, considerably smaller than the "average spacing" between the particles of the deuteron (4.31×10^{-13} cm). Most of the interactions with the incident neutron are thus of the "two-body" type, either n-p or n-n, leaving the third particle nearly unaffected. This is essentially the basis of the "impulse approximation" of Chew,[14] for which this and several other experiments provide a fair degree of justification. Using this approximation, Chew shows that if a collision occurs that tends to transfer considerable energy to both particles of the deuteron, i.e., at a time when the instantaneous spacing within the deuteron is of the order of the de Broglie wave length, then the deuteron shows a considerable

reluctance to break up. The collision then results in an elastic scattering which need not be considered here.

The major part of the kinematics, then, has been worked out in the previous section as free neutron-proton scattering. The small binding of the deuteron particles manifests itself principally in allowing small components of internal motion of the target particle at the instant of collision. This internal motion affects both the size and direction of β_c and so modifies slightly the values obtained from Table I. Components of this motion transverse to the direction of the incident neutron cause a deviation in angle from the values given, and components in the direction of the incident neutron cause an energy spread for the scattered particles. In addition, the small amount of energy carried off by the third particle decreases the average energy of the scattered particle from that predicted in the free n-p collision.

No effort is made in the present experiment to measure the angular spread or to separate out the contributions from other angles (due to this spread) to the counting rates at a given angle. The theory to which these data are to be compared has already included this effect in predicting differential cross sections. This theory also sums over the entire energy spectrum of particles scattered at a given angle, and the data must be treated accordingly for comparison.

The experimentally measured energy distribution of protons from the n-p type of inelastic collision is shown in Fig. 15. This is to be compared with the distribution given in Fig. 14 for protons from free n-p collisions at the same laboratory-system angle of scattering. The distribution shown in Fig. 15 is seen to be somewhat wider, and peaked at a slightly lower energy (about 6 Mev). as predicted in the discussion above. The major breadth, however, is still due to the energy spread of the incident neutrons rather than to the high-momentum components of internal motion at the instant of collision. These high-momentum components occur when the spacing between deuteron particles is small, and hence just when Chew predicts that elastic scattering will become the dominant effect.

III EXPERIMENTAL ARRANGEMENT

The Neutron Beam

The 90-Mev neutron beam is produced in the Berkeley cyclotron by the bombardment of a two-inch beryllium target with 190-Mev deuterons. A stripping process occurs, as described by Serber,[17] in which one of the particles in the deuteron collides with a beryllium nucleus while the other particle goes on almost unaffected. Those collisions in which the proton is captured give rise to a neutron beam coming off in a narrow cone tangential to the orbit of the deuterons. The angular divergence is due primarily to the components of internal momentum in the deuteron transverse to its path. Similarly, there is an energy spread caused by the internal-momentum components along the deuteron path. Both energy and angular distributions have been predicted by Serber and confirmed by various experimenters.[2,18] The peak of the energy spectrum occurs at 90 Mev and has a full width at half-maximum of 30 Mev. Actually, the present experiment provides one of the best measurements to date of the shape of the energy spectrum, as shown in Fig. 3.

The neutron beam was collimated to a rectangular cross section by means of an iron and brass neutron collimator constructed by Dr. Martin Stern and Mr. Robert Tripp. This collimator fits into an eight-inch diameter hole through the fifteen-foot concrete shielding, in the innermost of three five-foot concrete blocks. Thus, the collimation is provided well ahead of the experimental apparatus, which then has a very small solid angle for "seeing" charged-particle spray from the collimator. Two beam sizes are available at the exit side of the neutron hole; 3.50 in. vertical by 1.95 in. horizontal, or 2.70 in. vertical by 0.75 in. horizontal. In this experiment, the large beam was used with a CD_2 target and the small beam, reduced even further to a cross section of 1.50 in. by 0.75 in., was used with a liquid deuterium target. A plan view of the experimental arrangement is shown in Fig. 4.

Choice of Detection Method

One of the important phases in the early planning of an experiment in which particles of various masses are to be counted is the choice of the detection method that will provide the greatest mass resolution. Certain empirical relations, and curves derived from them, are very useful in this respect and have strongly guided the planning of this experiment. They are also used at various points in analyzing the data, and a brief resume of this subject is included here, even though excellent discussions can be found elsewhere (see especially York, UCRL-359).

Over a wide energy interval, there is a simple empirical relation between the range of a particle and its energy. Between 10 and several hundred Mev, the range-energy curve as given by Aron[19] for, say, a proton in aluminum is very nearly a straight line on a log-log plot. Thus a power law is indicated, with exponent measured as 1.76 in the region under discussion, with less than fifteen percent error incurred even at 1 Bev. Thus, the first relation of interest is:

$$R = K_1 E^{1.76} \qquad (1)$$

Furthermore, it is known experimentally that the specific ionization depends only on the velocity and the square of the charge of the incident particle. Thus one can write

$$\frac{dE}{dx} = K_2 Z^2 f(v^2) = K_2 Z^2 f\left(\frac{E}{m}\right) \qquad (2)$$

in the non-relativistic approximation.

Differentiation of thefirst relation to obtain dE/dx and elimination of the explicit energy dependence between this equation and (2) yields:

$$K_1 = \frac{1}{1.76\, Z^2 K_2 m^{0.76}} \quad \text{and} \quad f\left(\frac{E}{m}\right) = \left(\frac{E}{m}\right)^{-0.76}$$

Thus there results

$$\frac{dE}{dx} = KZ^2\left(\frac{m}{E}\right)^{0.76} \quad \text{and} \quad R = \frac{E^{1.76}}{1.76\,KZ^2 m^{0.76}}$$

Using other well-known relations to introduce various parameters, one can now plot these relations for various masses and charges to give a visual picture of the efficiency of various measurable laboratory quantities for particle separation. Such curves are shown as log-log plots in Fig. 5 with scale factors left arbitrary. Not only should the quantities chosen permit good separation between curves; they should also result in curves whose slopes assure the best possible experimental resolution for measuring the variables in question. Thus, in general, very flat or very steep curves should be avoided unless one can count on exceptionally good resolution for the slowly varying parameter. Other factors, equally important but depending upon the individual case, must be considered and the best compromise chosen.

In the present experiment it was felt desirable to avoid magnetic separation, if possible, because of the awkwardness involved in covering a large range of scattering angles without running either the neutron beam or the counters into the magnet yoke. Further problems of magnetic shielding for the phototubes and the difficulty in determining the effective solid angle for particles passing through a fringing field were discouraging even though the Hp vs. dE/dx method gives one of the best separations between protons and deuterons. The range methods were discarded for this experiment since it was desirable to count both protons and deuterons, simultaneously if possible to increase the efficiency of the data-collecting time. Velocity measurements seemed impractical since these involve a time-of-flight measurement necessitating a large distance between counter and target. It was anticipated that counting rates would be too low to allow the sacrifice in solid angle.

The method finally selected was the measurement of dE/dx and E of the scattered particles. From the curves of Fig. 5, one finds that the separation between masses is quite satisfactory for

this method. The slope of the curves is nearly unity so that, as shown by the boxes on the curve, resolutions of only fifteen percent in each counter are sufficient to give complete separation between protons and deuterons. Both masses record simultaneously and, in addition, one obtains a rather good measurement of the energy distribution for the particles.

The counter system and the method were first checked with neutron-carbon scattering. Pulses from the dE/dx and E counters were delayed by different amounts and placed on an oscilloscope sweep to be photographed on continuously moving film. Pulse heights were measured and distributions were plotted and analyzed. To speed up the data-reduction time in subsequent runs it was decided to display the data on the oscilloscope by using both directions of deflection: vertical deflections represented dE/dx values and horizontal deflections represented E values. The cathode ray tube was intensified only during the time of maximum excursion of the deflecting voltages, thus giving a bright dot whose position with respect to an origin mark is of significance. Many of these dots could then be photographed successively on a single frame of the film, producing a visual picture of the iso-mass hyperbolas expected from the power-law relation between dE/dx and E. The number of dots per frame in the actual data film had to be limited to prevent loss of counts due to excessive overlap of the dots. In order to read the data, it was necessary only to project the developed photograph onto a graph containing the iso-mass hyperbolas drawn to the proper scale and to count the dots falling in each mass group. Adjustment of the scale and the width of the distributions are discussed in Section IV. Figures 6a and 6b show a sample picture of the dots resulting from neutron-carbon collisions and a graph of the iso-mass hyperbolas.

Construction of Counters

The details of the counter construction are shown in Fig. 7. The first counter, an anthracene crystal 1 in. x 1 in. x 1/8 in., measures essentially the specific ionization of a high-energy charged particle. The crystal is mounted on a short lucite light pipe to allow

the desired geometrical position with respect to the back counter and also to insure more uniform light collection over the area of the crystal. Optical contact is maintained between the crystal and the photomultiplier by means of thin oil films at each of the surfaces. An aluminized glass mirror is held in optical contact with the edge of the crystal opposite the light pipe in order to increase the fraction of scintillation light seen by the photomultiplier.

The back counter is required to measure the energy that the charged particle has upon leaving the specific-ionization counter. A large sensitive volume is necessary for this measurement, and crystals therefore did not seem practical. Instead, a solution of terphenyl and diphenylhexatriene in phenylcyclohexane was chosen as the scintillator, thus allowing construction of the counter from lucite.

Several factors must be considered in deciding upon the size and design of the energy counter. Its minimum length is determined by the range of the highest energy proton that is to be measured, in this case about 120 Mev. Thus 11.1 cm is the minimum length for the counter; it was actually made 15 cm in length. The radius of the counter must be greater than the maximum lateral displacement caused by the angular acceptance of the counter and by the multiple scattering. For a two-inch target at 60 inches from the counters, the angular term amounts to 0.6 in. and the multiple-scattering term, using four times the rms lateral displacement calculated according to Eyges,[20] amounts to 0.17 in. for the worst case, the 120-Mev proton. The present counter was built with a 1-1/8 in. inside radius for ease of construction, and satisfies this requirement entirely.

To help insure uniform light collection over the entire length of the energy counter, the photomultiplier is separated from the liquid scintillator by a lucite plug of thickness equal to the radius of the counter. That this aids the uniformity can be seen in the following way: Light given off at the end of the counter farthest from the phototube will be collected by the tube only if it lies in the forward or backward cone of half angle measured to the counter axis equal to 45 degrees, the critical angle of reflection for a lucite-air surface.

For the best uniformity, one should thus strive to collect the same fraction of light produced in the end of the counter nearest the phototube. The lucite plug mentioned above causes the phototube to subtend just such a solid angle. An experimental check of the uniformity was made using the 1.3-Mev gamma ray from Na^{22}; results are shown in Fig. 8. A curve of counting rate vs. discriminator setting was obtained with the Na^{22} source placed just above the center of the energy counter. A steep portion of the curve was chosen as the operating region to insure maximum sensitivity, and discriminator readings necessary to maintain the original counting rate were taken as a function of position along the counter length. Several "runs" were taken in order to average out drifts in the electronics. Approximately two percent nonuniformity in pulse height was found for the end of the counter farthest from the phototube.

The two 5819 photomultiplier tubes used in the experiment were selected from a group of about 12 as having the best pulse-height resolution for the cesium^{137} gamma-ray spectrum. This selection is very important, as there is wide variation from tube to tube. Magnetic shields of soft iron were placed around each of the counters to prevent loss in pulse-height resolution due to the fringing field of the cyclotron at the position of the experimental setup.

Monitor

During the course of a run, the neutron beam fluctuates because of drifts within the cyclotron. Thus it is necessary to monitor the beam intensity continually in order to normalize data to the same number of incident neutrons. Also, in regions of low background or low cross section it is desirable to increase the beam intensity to speed up the data-taking process. For this experiment a monitor was used which indicates relative beam intensities only. It consists of a BF_3-filled proportional counter, constructed by Mr. Boyd Thompson, and placed in an auxiliary hole through the concrete shielding (see Fig. 4). This counter is sensitive only to low-energy

neutrons by means of the n-α capture cross section in B^{10}, and really monitors only the flux of such neutrons in the shielding near it. These neutrons are present, however, primarily through the slowing down of high-energy neutrons by collisions in the concrete, and depend markedly on beam strength.

A check was made on the proportionality of this monitor to the number of neutrons in the actual beam in the following way: A large ionization chamber belonging to Professor Wilson Powell of this laboratory, containing a number of thin sheets of polyethylene for efficient conversion of neutrons to charged particles, was placed in the direct neutron beam. Comparison was made between the integrated charge collected from the ionization chamber and the number of counts registered by the BF_3 counter for various beam levels as recorded on Zeus meter number 1 (an ionization chamber permanently attached to the yoke of the cyclotron and inside the concrete shielding). Results are shown in Fig. 9; the proportionality seems to be good to at least two percent over the range of beam intensity from 1/4 to 4 roentgens, as recorded on Zeus No. 1. It appears that above 4 r. the ionization chamber became saturated, causing an increase in the ratio of BF_3 counts to ion-chamber charge. Owing to the uncertainty of the proportionality above 4 r., operating levels were always selected at 3 r. or less.

Electronic Apparatus

A block diagram of the electronic circuit is shown in Fig. 10. Singles counting rates with the neutron beam are not great enough to require very fast electronics; the standard laboratory counting equipment could be used for the most part. A few special devices were necessary for the photographic method of recording the data, and these were designed and constructed with the aid of Mr. Leroy Kerth.

Voltage signals from the 5819 photomultiplier tubes were shaped immediately to two-microsecond, flat-topped pulses of heights proportional to the original signals by means of condensers and shorted RG 65/U clipping lines at the inputs of standard UCRL

pre-amplifier units. The amplified signals from each counter were then split and passed into two completely separate electronic circuits.

One pair of signals was used to provide an indication of counting rates and accidental coincidence rates at the time of operation so that these could be properly controlled. The beam intensity was maintained at such a level that the accidental rate was less than three percent of the coincidence rate at all times.

The second pair of signals was used for displaying the data on an oscilloscope for photographic recording. The pulses were passed into linear amplifiers having a gain of 10,000, through ladder attenuators and the amplifiers of the Tektronics 511 oscilloscope to the horizontal and vertical deflection plates. A second output from each of the linear amplifiers was used to form a coincidence in a special coincidence-intensifier unit. This circuit consists of a cathode-fed, Rossi-type coincidence unit, a Schmidt discriminator circuit, and a pulse shaping circuit designed by Dr. Richard Post. It delivers a 0.3-microsecond negative pulse of definite height to the cathode of the cathode ray tube as an unblanking voltage, and also provides a positive pulse of slightly greater length for energizing a scaler. A variable delay control allows adjustment of the timing of these pulses so that the oscilloscope will be unblanked only during the time of maximum excursion of the deflection voltages. The resulting flashes of light were recorded on Kodak 35 mm Linograph Pan film with the aid of a General Radio oscillograph recorder having an f/1.5 lens. In order to obtain the necessary intensity to make the photographic process possible, a Tektronix 511 oscilloscope was modified with a 5XP11A cathode-ray tube operating at 15 kev. An aluminized tube face was necessary to prevent filament glow from recording on the film.

To prevent excessive overlap of the dots it was found desirable to change frames on the film every 64 counts. On the average, this number of counts occurred in about 90 seconds, so it was necessary to provide a rapid frame-changing device to make running time more efficient. A count-control unit was devised by modification of an existing circuit designed by Mr. Leroy Kerth. A Decade Telephone Stepping Relay was activated by the register pulse of the intensifier

scaler and counted off any number of such pulses between one and ten as selected by a front panel control. This control, in combination with the scaling factor of the intensifier scaler, allowed a wide selection in the number of pulses to be recorded on a frame. When the selected number had been attained, the intensifier and all scalers were automatically disabled and the camera motor was energized to move the film to the next frame. At the end of the motion an origin mark was placed on the film to indicate the zeros of the deflection system, and the disabling voltages were removed from the scalers and intensifiers. The entire operation required only two seconds, and thus satisfied the efficiency requirement. The horizontal and vertical deflection directions were designated on the film occasionally to check for changes in alignment by manually applying the scope sweep voltage to the horizontal or vertical input terminal of the oscilloscope.

Scaler data were recorded only every 25 frames, so that it was thought desirable to record "on-off" times for each frame to allow correction of the monitor in case any frame in the set of 25 had to be discarded. A Simplex Productograph Timeclock was used for this purpose, receiving energizing signals at the proper times from the count-control unit.

Scattering Targets

1. Deuterated wax target

The first runs of this experiment were made using deuterated wax for a scatterer. A $(CD_2)_n$-C difference is then necessary to separate out the pure n-D effect. A third target, of $(CH_2)_n$, then allows a simple means of normalizing the data to the accurately known differential cross section for n-p scattering at 90 Mev.[2] The n-p data were also used to good advantage in calibrating the experimental equipment, as discussed in Section IV.

The $(CD_2)_n$ target contained 9.10 g of material, presenting an area to the beam of 3.15 cm by 4.38 cm, or 13.80 sq. cm. The carbon and $(CH_2)_n$ targets were made to the same area and of the proper number of grams per cm^2 to give the same energy loss by

charged particles as the $(CD_2)_n$ target. In normalizing the counting data, one must multiply the carbon counts by the factor 0.710 in comparing to $(CD_2)_n$ and by 0.698 in comparing to $(CH_2)_n$. The ratio of hydrogen atoms in the $(CH_2)_n$ to deuterium atoms in the $(CD_2)_n$ was 0.981.

In making angular changes, the targets were rotated in the beam to the same angle as the counters so that the thinnest dimension of the target was always presented to the counters. The neutron beam was large enough in size to completely cover the target at all angles of measurement.

2. Liquid deuterium target

The charged-particle background caused by the carbon in the CD_2 target was appreciably large; for example, the carbon contributed more than twice as many deuterons as the elastic n-D scattering effect being measured. It was thus very difficult to obtain satisfactory statistics on the deuteron effects without using excessive amounts of cyclotron time.

A liquid deuterium condenser and target system designed by Mr. Roscoe Byrns and Mr. Warren Chupp was ideally suited to this experiment and was generously lent for use here. (Details of the construction and operation of the system are to be presented in a separate paper by Mr. Chupp and Mr. Byrns; only a brief description of its operation is given here.) A schematic diagram of the system is presented in Fig. 11 and a photograph of the condenser in position in the neutron beam is given in Fig. 12. Liquid hydrogen, contained in a six-liter vessel surrounded by heat shields maintained at liquid-nitrogen temperature, is used as coolant in an efficient heat-exchange system with the incoming deuterium gas. The boiling point of deuterium is nearly 3.5° Kelvin higher than that of hydrogen in the vicinity of one atmosphere pressure, so that the condensation process takes place very readily if the target and last section of heat exchanger are maintained near liquid hydrogen temperature.

The measured pressure over the liquid deuterium indicated that the termperature of the system was truly that of liquid hydrogen,

so that it was possible to condense hydrogen gas in the target by application of only two pounds positive pressure. Thus it was possible to normalize the deuterium data to the hydrogen data for cross-section calculations, as was done with the wax targets. Background runs were made for each scattering angle while the target and condenser system were evacuated.

In order to compare data from the liquid deuterium with data from the liquid hydrogen it is necessary to know the ratio of the number of atoms of each present in the target. An empirical relation has been worked out[24] for the molar volume of liquid deuterium in the temperature region of 19.5° to 24.5° K. For the liquid hydrogen boiling point at atmospheric pressure, 20.6° K, one finds for the molar volume of liquid deuterium: 0.0422 mols/cm^3. From the density of liquid hydrogen at atmospheric pressure[25] the molar volume is found to be 0.0352 mols/cm^3. The ratio of the number of atoms of hydrogen to the number of atoms of deuterium is then:

$$\frac{H_2}{D_2} = 0.834$$

The actual target consisted of a three-inch diameter brass cylinder of 1/8 in. wall thickness and 1.25 in. in length. The ends through which the beam passed were covered with 5-mil brass foil, preformed into spherical sectors giving a target thickness of 1.80 in. at the center. In addition, the neutron beam passed through two aluminum heat shields of two mils each and through two stainless steel vacuum jacket foils of five mils each.

Because of the small size of the target, it was necessary to use the smaller of the two neutron collimators, reduced even further, to provide a beam 2 cm by 4 cm in cross section at the position of the target. The high-energy x-rays present in the neutron beam were used to give a photographic indication that the target was centered on the beam. It is essential to avoid scraping of the beam with the three-inch diameter brass cylinder, as excessively high backgrounds would result.

An analysis was performed on the deuterium gas by Dr. Amos Newton, using a mass-spectrograph method. The composition of the gas was reported as: 98.6 percent D_2, 0.54 percent HD, 0.84 percent He, and no detectable quantities of N_2, O_2, or CO_2.

Since the helium does not condense at liquid hydrogen temperatures, contamination in the liquid phase is due to HD only and is reduced from the above ratio of HD to D_2 by the ratio of the vapor pressures of the two liquids at liquid hydrogen temperature, 20.6° K. Thus, only 0.28 percent of the liquid is HD and only 0.14 percent of the atoms present in the target are hydrogen contaminant.

Even with the smaller effective area available in the liquid target, more than twice as many deuterium atoms were presented to the beam as were available in the wax target. In addition, the ratio of deuterium to background atoms is improved by something more than a factor of ten.

Geometry and Angular Resolution

In both target systems described above, the counters were rigidly attached to the target platform and the entire assembly was rotated about the midpoint of the scatterer in making angular changes. The specific ionization counter was the defining area for solid angle and angular resolution and was placed 60 in. from the target in both cases. The angular resolution determined from the geometry alone amounts to ± 1-1/4 degrees. Multiple scattering by the target and foils increases this to 2.1° for protons at 5°, 3.0° for protons at 40°, 2.3° for deuterons at 5°, and 3.3° for deuterons at 40°.

A large proportion of the target-out counting rate was found to be caused by collisions of the neutron beam with air molecules in its path. Proper shielding of the counters from all the air path except the immediate vicinity of the target reduced the target-out counts to about one fourth of the unshielded rate.

Experimental Procedure

1. Alignment of the experimental apparatus in the neutron beam

Crosshairs define the center of each end of the neutron collimator; it is possible to establish the beam line with some accuracy by alignment of a cathetometer on the crosshairs. The two-inch beryllium stripping target is then placed in position inside the cyclotron tank so that the leading edge is centered in the field of view. An x-ray film, loaded in a film holder coated with zinc sulfide, is placed behind the cathetometer and is exposed for ten minutes to the full intensity neutron beam. Enough x-rays are present in the beam to provide an excellent picture of the alignment of the cathetometer. After this check, the remainder of the experimental equipment can be set up along the line of sight of the telescope. Experience has shown that the 80.7-inch radius is the proper location for the beryllium target and the exit position of the beam is then quite reproducible from run to run.

2. Adjustment of the electronics

Several precautions must be observed in adjusting the electronic equipment. A pulser, giving two-microsecond pulses similar to those produced by the phototubes and pulse shapers, is fed into the amplifier system, which is operating at maximum gain. The input level to the amplifiers is increased until saturation of the output is just noticeable on the oscilloscope. The attenuators on the oscilloscope amplifier inputs are then adjusted to place this saturation level at four centimeters deflection, the maximum available in the vertical direction on a 5XP11 cathode-ray tube. The input attenuator on the "sweep amplifier" of the oscilloscope was found to be frequency dependent, changing the shape as well as the height of the pulses, so a UCRL ladder attenuator was substituted in its place.

The pulser output level was then reduced and the pulses from the two amplifier systems displayed simultaneously on the oscilloscope, producing a lissajou pattern shaped like a jumping porpoise.

The timing of the intensifier spot was then adjusted so that it fell on the nose of the porpoise, since this represents the maximum excursion of the two deflections.

The pulser was then replaced by the counter system, in counting position, and phototube voltages were adjusted to give deflections from real counts covering the entire four centimeters in each direction. A few photographs were made with five times the usual number of pulses to give a visual picture of the proton and deuteron distributions. The mass resolution can be checked in this way, and one can also be sure that the entire useful pulse height is being displayed in each direction. Such "burned-in" pictures were taken occasionally and developed immediately to provide a continual check on the equipment during the course of a run.

Final data were read from the film by projecting in a Recordak Microfilm Viewer having a magnification factor of 19. The oscilloscope camera had been focussed at such a distance that the four-centimeter deflections just covered the normal 35 mm frame. Thus, the overall magnification of the optical system was 7.5, providing considerable ease in reading the dot data.

IV CALIBRATION OF THE EQUIPMENT

It was decided to establish as objective a method as possible in separating the deuterons from the protons on the film data, since the division into two groups was not absolute. Using range and specific-ionization curves for anthracene and phenylcyclohexane, calculated from the values given by Aron[19], one can compute energy losses in the two counters for various values of incident proton and deuteron energies. The calculation can be extended to other mass values by using the equations of Section III, page 12. (See Appendix A.) In this way, energy-loss values were obtained for each 0.1 proton mass unit between 0.4 and 3.0 units. In order to use these values in obtaining experimental mass distributions, it was then necessary to obtain for each counter a scale factor relating the energy lost in the counter to the deflection observed on the projected picture.

To obtain the scale factor, dE/dx and E distributions were measured on an arbitrary scale for particles scattered at a given angle Φ into the counter system by free n-p collisions. The peak of the neutron beam spectrum, known from other measurements to occur at 90 Mev, was then related to the peaks of the measured spectra by $E \cos^2 \Phi$ and the corresponding dE/dx values given by Aron[19] for protons. Measurements were made for several angles of scattering to provide calibration for various energies. Typical measured distributions are shown in Figs. 13 and 14, along with points for the neutron spectrum predicted from the Serber theory of deuteron stripping.

A check was also made on the nonlinearities of the amplifier system by measurement of the dot positions resulting from a pulser-and-attenuator system. This correction and the measured scale factors were applied to the calculated energy-loss values and iso-mass curves drawn to the scale of the projection system. The mass distribution for particles knocked out of carbon at ten degrees to the neutron beam was measured from these curves with the results shown in Fig. 16.

A Gaussian curve was fitted to the proton data and found to give a very good representation of the shape. If one assumes that this Gaussian spread is due entirely to statistical fluctuations in the number of photoelectrons collected by the cathodes of the photomultiplier tubes, a simple argument shows that for a particle of different mass, m, and average energy E_m one should have a Gaussian width related to the proton width by:

$$\sigma_m = \sigma_p \left(\frac{m}{m_p}\right)^{0.62} \cdot \left(\frac{E_o}{E_{op}}\right)^{0.38} \qquad \text{(See Appendix B)}$$

For deuterons, which have, at a given scattering angle, an energy 8/9 that of a proton, this ratio is 1.47. The curve through the deuteron group of Fig. 16 has this width and is seen to be only slightly too narrow.

It is seen also in Fig. 16 that the protons have a measured mass of 0.89 and the deuterons a mass of 1.58. The low values can probably be adequately explained in the following way:

It is well known that for very large values of specific ionization a scintillating substance can no longer respond proportionally to the energy lost in the substance. Since the particles actually are stopped in the energy counter of the present system, the specific ionization becomes very large near the end of the range, producing this saturation effect. The measured energy value is thus lower than the value expected from the energy-loss calculations. The method used in finding the scale factors was insensitive to the small additive term in question.

The following evidence is offered for the plausibility of this explanation:

It is shown in Appendix C, on the basis of the assumption that saturation occurs suddenly, that the energy correction for deuterons is just twice the correction for protons. The values measured from the iso-mass curves are indeed 8 Mev to bring the mass 0.89 line to 1.00 and 16 Mev to bring the mass 1.58 line to 2.00.

Furthermore, it is shown in Appendix C that the saturation value of dE/dx can be calculated from these energy-correction data. A value of 29 Mev/g · cm^{-2} is obtained for phenylcyclohexane. Fig. 17 compares the saturation effect calculated here for the liquid scintillator with experimental data on the saturation effect in anthracene[21]. The agreement seems sufficiently good to justify the explanation of the low mass values.

In reading the final data from the film, it was decided, on the basis of the Gaussian nature of the distributions of Fig. 16, to count as protons only those particles lying between mass 0.75 and mass 1.05 and as deuterons those between mass 1.30 and mass 2.10. Using Gaussian widths of 0.13 and 0.20 for the two groups, one finds that these criteria include 75.0 percent of the area of the proton group and 91.5 percent of the area of the deuteron group. Cross contamination of the mass groups was virtually eliminated by this choice of cutoffs.

It was necessary to read mass distributions at each of the angles of scattering, since the width of the distribution was found to vary slightly with the average energy of the particles being counted. This effect is, in fact, predicted in the calculation of Appendix B. The same mass cutoff values were used for all angles of scattering, but the fraction of the total distribution counted between these limits changed slightly with angle and had to be taken into account in the reduction of the data.

Low-energy cutoffs were calculated for protons and for deuterons at each angle of scattering, with energy losses in the target and air path included, so that only the effects of neutrons having an energy greater than 60 Mev were measured. This criterion was established by Hadley et al[2] in measuring the n-p cross sections to which the present data are normalized.

V REDUCTION OF DATA AND CORRECTIONS

General Formulae for Cross Sections

From the usual formula for the cross section, one has for the total number of counts obtained at the laboratory angle, Φ, and in the solid angle, $\Omega_{lab.}$:

$$C(\Phi) = N_n N_t (\Phi) \left[\frac{d\sigma}{d\Omega}(\theta)\right]_{cm} \left[\frac{d\Omega_{cm}}{d\Omega_{lab.}}\right]_{\Phi} \Omega_{lab.}$$

where:

$\left[\frac{d\sigma}{d\Omega}(\theta)\right]_{cm}$ is the differential cross section in the center-of-mass system at angle θ,

$N_t(\Phi)$ is the number of target nuclei in the beam when measuring at the laboratory angle, Φ,

N_n is the total number of neutrons which pass through the target during the measurement and is equal to a constant, K', times the monitor count.

But by measuring the ratio between events produced in an n-p scattering process and the monitor count obtained during this time one can apply the above equation to find the product, $K' \cdot N_p(\Phi) \cdot \Omega_{lab}$ in terms of the known n-p scattering cross section at 90 Mev.[2] Defining this product as $K(\Phi)$, one then has for any other reaction:

$$\left[\frac{d\sigma}{d\Omega}(\theta)\right]_{cm} = \frac{C(\Phi)}{Mon.} \cdot \frac{1}{K(\Phi)} \cdot \frac{N_p(\Phi)}{N_t(\Phi)} \cdot \left[\frac{d\Omega_{lab}}{d\Omega_{cm}}\right]_{\Phi}$$

or $$\left[\frac{d\sigma}{d\Omega}(\Phi)\right]_{lab} = \frac{C(\Phi)}{Mon.} \cdot \frac{1}{K(\Phi)} \cdot \frac{N_p(\Phi)}{N_t(\Phi)}$$

Sample Calculation of Cross Sections from Experimental Data

A sample calculation is here carried through for data taken by the CD_2-C difference method, since this is the most cumbersome case. The liquid dueterium case is almost identical except that the carbon subtraction is not required. Table II gives sample data at 25^o from the wax targets.

Table II

Data at 25°:

Target	C_p	C_d	Mon	C_p/Mon	C_d/Mon
CH_2	1202	214	1818.4	0.661 ± 0.019	0.118 ± 0.008
C	1154	544	3937.7	0.294 ± 0.009	0.138 ± 0.006
CD_2	2641	726	5194.7	0.510 ± 0.010	0.140 ± 0.005
none	220	109	2049.2	0.107 ± 0.007	0.053 ± 0.005

Counted protons in only 75.0% of mass distribution.
Counted deuterons in only 91.5% of mass distribution.
Ratio of carbon in CH_2 to carbon in C target 0.698
Ratio of carbon in CD_2 to carbon to C target 0.710
Ratio of hydrogen in CH_2 to deuterium in CD_2 0.981

Then:

(1) $$\text{Protons/Mon from } H_2 = \frac{1}{0.750}\left\{\left[\left(\frac{C_p}{\text{Mon}}\right)_{CH_2} - \left(\frac{C_p}{\text{Mon}}\right)_{\text{none}}\right] - 0.698\left[\left(\frac{C_p}{\text{Mon}}\right)_{C} - \left(\frac{C_p}{\text{Mon}}\right)_{\text{none}}\right]\right\} = 0.565 \pm 0.027$$

(2) $$\text{Deuts./Mon from } H_2 = \frac{1}{0.915}\left\{\left[\left(\frac{C_d}{\text{Mon}}\right)_{CH_2} - \left(\frac{C_d}{\text{Mon}}\right)_{\text{none}}\right] - 0.698\left[\left(\frac{C_d}{\text{Mon}}\right)_{C} - \left(\frac{C_d}{\text{Mon}}\right)_{\text{none}}\right]\right\} = 0.0066 \pm 0.0092$$

(3) $$\text{Protons/Mon from } D_2 = \frac{1}{0.750}\left\{\left[\left(\frac{C_p}{\text{Mon}}\right)_{CD_2} - \left(\frac{C_p}{\text{Mon}}\right)_{\text{none}}\right] - 0.710\left[\left(\frac{C_p}{\text{Mon}}\right)_{C} - \left(\frac{C_p}{\text{Mon}}\right)_{\text{none}}\right]\right\} = 0.360 \pm 0.016$$

(4) $$\text{Deuts./Mon from } D_2 = \frac{1}{0.915}\left\{\left[\left(\frac{C_d}{\text{Mon}}\right)_{CD_2} - \left(\frac{C_d}{\text{Mon}}\right)_{\text{none}}\right] - 0.710\left[\left(\frac{C_d}{\text{Mon}}\right)_{C} - \left(\frac{C_d}{\text{Mon}}\right)_{\text{none}}\right]\right\} = 0.0296 \pm 0.0073$$

From (1): $\frac{1}{K} = \frac{\left[\frac{d\sigma}{d\Omega}\ (159.5^{o})\right]_{n\text{-}p,\ cm}}{(\text{Protons/Mon})_{H_2}} \cdot \frac{d\Omega_{cm}}{d\Omega_{lab}}\ (\Phi = 25^{o})$

where $\left[\frac{do}{d\Omega}\ (159.5^{o})\right]_{n\text{-}p,\ cm} = 6.5_5$ mb/ster.

and $\frac{d\Omega_{cm}}{d\Omega_{lab}}\ (\Phi = 25^{o}) = \frac{1}{0.268}$ according to reference (2).

$$\therefore \frac{1}{K} = \frac{6.5_5}{0.565 \times 0.268}$$

$$= 43.3 \pm 2.1 \text{ mb. ster.}^{-1} \left(\frac{\text{Counts}}{\text{Mon}}\right)^{-1} \cdot \left(\frac{\text{Target Nuclei}}{CH_2\ \text{Proton}}\right)$$

Then, for elastic n-D scattering, using (4):

$$\left[\frac{d\sigma}{d\Omega}\ (129.5^{o})\right]_{cm} = 0.0296 \times 43.3 \times 0.981 \times 0.274$$

$$= 0.34_2 \pm 0.08_8 \text{ mb./ster.}$$

For inelastic n-D scattering, using (3):

$$\left[\frac{d\sigma}{d\Omega}\ (25^{o})\right]_{lab.} = 0.360 \times 43.3 \times 0.981 = 15.3 \pm 1.0 \text{ mb./ster.}$$

For an upper limit on n-p radiative capture, using (2):

$$\left[\frac{d\sigma}{d\Omega}\ (25^{o})\right]_{lab.} = 0.0066 \times 43.3 = 0.29 \pm 0.40 \text{ mb./ster.}$$

Corrections for Elastic Scattering Data

The cross sections for elastic scattering were normalized by comparing the number of deuterons per monitor count from a deuterium target with the number of protons per monitor count from a hydrogen target. Owing to the difference in mass between the measured particles, several possible correction factors must be considered.

A loss of particles is expected in the method used for the present measurement because of nuclear interactions in the energy counter. If a nuclear event occurs, some of the energy of the incident particle escapes detection through the emission of neutral particles in the collision. A particle is then recorded on the photographic film with the proper specific ionization from the first counter but with a reduced energy in the second counter. If the loss is sufficiently great, the particle is thrown out of the mass band being counted and is lost from the data. A resonable estimate of the loss can be calculated using the absorption cross sections of Kirschbaum[26] for protons and the total inelastic cross sections of Crandall[27] for deuterons. The assumption was made that one-half the energy of the incident particle at the time of the collision was lost to neutral particles, and an empirical relation was measured from the iso-mass curves for the energy loss necessary at each position to throw the particle out of the mass group being counted. A numerical integration was carried out over the spectrum of particles scattered at the angle Φ, using the opaque-nucleus equation of Serber[17] for the neutron energy spectrum. The loss of protons was found to vary from 4.0 percent at 5° scattering angle to 1.4 percent at 40°; deuteron losses vary between 4.3 percent at 5° and 0.8 percent at 40°. The correction factor needed is the ratio of protons to deuterons which do not undergo such collisions. This ratio varies between 1.01 at 5° and 0.99 at 40°. There is a negligible contamination of the protons from inelastic n-D scattering caused by the nuclear interactions of the elastically scattered deuterons.

Additional losses of the scattered particles result from nuclear interactions in the target material, air path, and first counter. Again using the cross sections of Kirschbaum and Crandall, one finds a 0.9 percent loss of protons and a 2.1 percent loss of deuterons. The correction factor for particles counted is 1.01.

Multiple scattering of particles in the first counter does not result in a loss of counts since the back counter is large enough to include particles scattered by as much as four times the rms scattering angle. Multiple scattering in the target and foils broadens the angular resolution but does not contribute to the loss of particles.

As mentioned previously, only scattering events produced by neutrons of energy greater than 60 Mev were counted. At large angles of scattering, however, the calculated cutoff for deuterons fell below the electronic cutoff of the coincidence-intensifier unit. It was thus necessary to correct the measured data by the factor relating the total number of neutrons in the beam with energy greater than 60 Mev to the number with energy greater than the value calculated from the electronic cutoff. To calculate this factor, the energy thickness of the target, as a function of scattering angle and neutron energy, was folded with the neutron spectrum of Serber for the opaque nucleus. The resulting curve for each angle was numerically integrated above 60 Mev and above the neutron energy corresponding to the electronic cutoff for that angle. The ratio of these areas is the correction factor to be applied. For an angle of 40° it was necessary to calculate a similar correction for the scattered protons. The principal error in the calculation is the assumption that the scattering cross section is independent of neutron energy over the region between 60 Mev and the electronic cutoff value.

Corrections for Inelastic Scattering Data

The corrections for inelastic scattering are much simpler than for elastic scattering, as there is no mass effect to be accounted for in the normalization process. There is, however, a correction to be applied in connection with the low-energy cutoff. Because of the three-body nature of the inelastic scattering problem, it is impossible to calculate a cutoff value. The following procedure was employed instead:

The same low-energy cutoff was used for the inelastic n-D events as was used for the free n-p scattering. An energy spectrum for the protons coming from the inelastic scattering was measured, as in Fig. 15, and the fraction of the total area under the curve lying above the cutoff was obtained. A similar measurement was carried out for protons scattered at the same laboratory angle from free n-p collisions. The values of the inelastic n-D cross sections obtained from the raw data were then multiplied by the ratio of these fractional areas to normalize the n-p and n-D effects to the same percentage of the total neutron beam spectrum.

Discussion of Errors

In addition to the statistical errors which can be calculated for the data, the possibility of certain systematic errors should be mentioned and the errors estimated. The most important ones are as follows:

1. The consistency of the response of the monitor to fluctuations in beam level was checked only to the order of two percent.

2. The ratio of the number of deuterium atoms to the number of hydrogen atoms in the liquid target is uncertain to a few percent, because of bubbles from the boiling of the liquid. As both liquids were maintained at their equilibrium pressures it is probable that the boiling rates were very nearly equal.

3. There is an uncertainty, probably of the order of ten percent, in the factors used to obtain the total areas under the mass gaussians for deuterons at the large scattering angles. There were too few deuterons present to obtain better values for the distribution widths.

4. There is an uncertainty of about five percent in the correction for the low-energy cutoff, caused by the electronics. This correction is applicable only at large angles of elastic scattering.

5. The low-energy cutoff correction for inelastic scattering is uncertain to about five percent, (but is applicable for all angles of scattering).

6. The absolute value of the neutron-proton scattering cross section used in normalizing the present data has an uncertainty given by Hadley, et al[2] as ± ten percent.

The data are tabulated and plotted with only the statistical uncertainties given, but the systematic errors must be considered in comparing these with the data from other experiments.

VI FINAL RESULTS AND CONCLUSIONS

The corrected results for elastic scattering are listed in Table III. The data obtained from the CD_2 target and from the liquid deuterium target are listed separately for comparison. The data of Stern[10] are also tabulated for comparison. The weighted averages of the present data are plotted in Fig. 19 along with the data of Stern and the calculated curves of Chew[14] and of Horie, Tamura, and Yoshida.[22]

In Table IV are given the results for inelastic scattering. These are compared with the data obtained by Hadley[23] for the n-p type of inelastic scattering of 270-Mev neutrons by deuterons. Figure 20 compares the present results with the theoretical predictions of Chew.[15].

The relative cross sections for n-p scattering, as measured in the present experiment, are shown in Fig. 18. The data were normalized to give the best fit to the curve of Hadley et al.[2] The low value at 5^o is thought to be caused by a loss in efficiency in counting the dots in the region of small dE/dx and large E, where the oscilloscope focus was not good.

Table III

θ	CD_2-C	Liquid D_2	Stern
169.8^o	--	2.80 ± 0.22	1.75 ± 0.34
159.7^o	1.54 ± 0.45	1.41 ± 0.08	1.52 ± 0.20
149.5^o	1.16 ± 0.19	0.86_5 ± 0.06	0.61 ± 0.06
139.4^o	--	0.64 ± 0.05	0.40 ± 0.05
129.3^o	0.35 ± 0.08	0.40 ± 0.05	0.55 ± 0.04
119.3^o	0.44 ± 0.10	0.23 ± 0.06	0.52 ± 0.09
109.2^o	--	0.26 ± 0.06	0.61 ± 0.05
99.1^o	--	0.41 ± 0.16	0.64 ± 0.05

Table IV

ϕ	CD_2-C	Liquid D_2	Hadley 270 Mev.	
5^o		0.55 ± 0.02	4^o	0.72 ± 0.02
10^o	0.50 ± 0.06	0.59 ± 0.02	9^o	0.68 ± 0.04
15^o	0.64 ± 0.06	0.64 ± 0.02	15^o	$0.75 \pm 0.04_5$
20^o	--	0.65 ± 0.02	-	--
25^o	0.63 ± 0.04	0.63 ± 0.02	$22\text{-}1/2^o$	$0.71_5 \pm 0.05$
30^o	0.68 ± 0.05	0.59 ± 0.02	30^o	0.83 ± 0.06
35^o	--	$0.50 \pm 0.01_5$	35^o	0.81 ± 0.11
40^o	--	$0.44 \pm 0.01_5$	45^o	0.64 ± 0.10

In discussing the results for elastic scattering, two angular regions are considered separately. In the region between 130^o and 180^o the pickup process of deuteron formation gives rise to the increase in cross section observed. The cross section in this region is also quite sensitive to the presence of tensor terms in the nuclear force, as can be seen in Fig. 19. Chew[14] used central forces only in an impulse approximation calculation, while Horie, Tamura, and Yoshida[22] included tensor forces in a Born approximation calculation. In this angular region the present data agree quite well with the data of Stern for 190-Mev deuteron-proton scattering. The disagreement at 170^o is not thought to be significant; the value obtained in the present experiment is probably ten percent high due to the low value obtained for the n-p scattering cross section at this angle (5^o point of Fig. 18) and subsequently used in the normalization.

In the angular region between 100^o and 130^o the present data seem to fall consistently below the results of Stern. Systematic errors may explain the discrepancy, although a factor of nearly two is necessary to bring these data into agreement with Stern's results.

The general agreement in shape and in magnitude between these two experiments is taken as further indication that a charge-independent theory of nuclear forces is justified at high energy as well as at low. It would perhaps be worth while to investigate the observed discrepance in the 100° to 130° region by a different method. A measurement of the cross sections in the region of small-angle scattering would also be of interest as a further check on the theory of charge independence at high energy.

For inelastic scattering Chew has calculated cross sections using the impulse approximation and the experimentally determined cross sections for free-particle scattering. For the n-p type of inelastic collision the theory predicts cross sections almost identical with the free n-p case except in the forward direction, where the action of the Pauli principle on the two residual low-energy neutrons impedes the reaction. The dotted curves of Fig. 20 show the limits between which the experimental data should lie. Clearly, there is considerable disagreement between the measured and predicted values. Instead of approaching the free n-p cross sections at large scattering angles, the present data retain an almost constant ratio to the free particle values of 0.5 to 0.6. Results similar to this were obtained for 270-Mev neutron-deuteron scattering by Hadley,[23] who found a ratio of 0.7 to 0.8. At the higher neutron energy it is reasonable that the collision should be more nearly a free-particle event, and the higher ratio is to be expected.

VII. ACKNOWLEDGMENTS

It is a pleasure to express my appreciation to Dr. Chaim Richman for the opportunity of doing my graduate research under his direction, and for the many occasions on which he has offered encouragement and suggestions during this period. I also wish to thank Dr. Burton Moyer for the interest he has shown in this experiment and for his part in making the liquid deuterium target available to us.

This entire work was carried out in cooperation with Mr. Leroy Kerth, whose assistance was invaluable to its success. Many of the electronic techniques were contributed by Mr. Kerth, as well as a great deal of hard work on the other phases of the experiment, at all hours of the day and night. Other members of Dr. Richman's group have contributed generously of suggestions and assistance whenever called upon, and it is a pleasure to thank them here.

I am indebted to Miss Irene d'Arche for assistance with the calculations and to Mrs. Beverly Baldridge and to my wife, Bernice, for help in reading the film data; to Mr. Warren Chupp and Mr. Roscoe Byrns for the use of the liquid deuterium target and for their assistance in its operation. I also wish to thank Mr. James Vale, Mr. Lloyd Houser, and the crews of the 184 inch cyclotron for their help and cooperation.

This work was performed under the auspices of the Atomic Energy Commission.

APPENDIX

A. Calculation of Iso-Mass Lines

Over a very large range of energies (3 Mev to 1 Bev for protons) there is an empirical relation between the range of a particle and its energy: $R = K \frac{E^{1.76}}{m^{0.76}}$

Using this relation, an equation can be derived for the energy lost in the specific ionization counter of the present experimental arrangement by a particle of mass m which stops in the energy counter with a loss of energy E_o.

In the traverse of the first counter, the residual range of the particle changes by an amount

$$Ri - Ro = \frac{K}{m^{0.76}} (E_i^{1.76} - E_o^{1.76}) = t$$ where R_i and E_i are the range and energy of the particle incident on the first counter, and R_o, E_o refer to the same quantities for the particle as it enters the energy counter; "t" is the thickness of the specific ionization counter.

Thus we have

$$E_i = \left[E_o^{1.76} + m^{0.76} \frac{}{K} t \right]^{\frac{1}{1.76}}$$

and

$$\Delta E = E_i - E_o = \left[E_o^{1.76} + \frac{m^{0.76}}{K} t \right]^{\frac{1}{1.76}} - E_o$$

To evaluate K, we use the "energy thickness" of the first counter to protons, as computed from the Range-Energy Tables of Aron.[19] That is, for an incident proton having just enough energy to pass through the first counter,

$E_o = 0$ and therefore $\Delta E_R = \left[\frac{m_p^{0.76}}{K} t \right]^{\frac{1}{1.76}}$

In the present case, a 1/8 inch anthracene crystal was used, so $E_{i_R} = 19.4$ Mev.

Thus $\frac{m_p^{0.76}}{K} t = (19.4)^{1.76} = 184.7$

And for a particle of mass m,

$$\Delta E = \left[E_o^{1.76} + 184.7 \left(\frac{m}{m_p}\right)^{0.76} \right]^{\frac{1}{1.76}} - E_o \quad .$$

This relation was checked for a deuteron, mass 2, against the value obtained from the table of Aron and was found to be in agreement.

B. Width of the Resolution Curve in a Mass Measurement by the Method of dE/dx and E

The efficiency of a scintillation counter system can be expressed in terms of the number of photoelectrons collected at the photocathode of the multiplier tube per Mev of energy lost by a particle in the scintillator. Define this number as "n". Then in the first counter of the present system a particle losing ΔE Mev delivers $n_1 \cdot \Delta E$ photoelectrons to the cathode of the first tube and the subsequent loss of energy E_o Mev in the second counter delivers $n_2 \cdot E_o$ photoelectrons to the cathode of the second tube. The collection process is subject to random fluctuations measurable by the usual rules for standard deviation.

Thus one measures, for counter No. 1: $(n_1 \cdot \Delta E) \pm \sqrt{n_1 \cdot (\Delta E)}$

and for counter No. 2: $(n_2 \cdot E_o) \pm \sqrt{n_2 \cdot E_o}$

The relative widths of the resolution curves are then:

$$r_1 = \frac{1}{\sqrt{n_1 \cdot \Delta E}} \quad \text{and} \quad r_2 = \frac{1}{\sqrt{n_2 \cdot E_o}}$$

Now, using the relation derived in Section III,

$$\frac{dE}{dx} \propto \left(\frac{m}{E}\right)^{0.76}$$

and adding the approximation that

$$\frac{dE}{dx} = \frac{\Delta E}{t}$$ where "t" is the thickness of the first crystal,

one finds: $$m \propto E \cdot (\Delta E)^{1.3}$$

Then the relative width of the mass resolution curve is:

$$r_m = \sqrt{r_E^2 + r_{(\Delta E)}^{2\ 1.3}}$$

But: $r_{(\Delta E)}^{1.3} = 1.3\ r_{(\Delta E)}$

So: $r_m = \sqrt{r_E^2 + 1.69\ r_{(\Delta E)}^2}$ and $\sigma_m = m\sqrt{r_E^2 + 1.69\ r_{(\Delta E)}^2}$

If one assumes that all of the statistical width of the E and ΔE measurements are due to the collection statistics for the photoelectrons, then: $r_E = r_2$ and $r_{\Delta E} = r_1$

$$\text{so} \quad \sigma_m = m\sqrt{\frac{1}{n_2 E_o} + \frac{1.69}{n_1 \cdot \Delta E}}$$

Now for the particles in question, E_o is about twenty times ΔE. The quantity n_1 will be approximately twice as large as n_2 due to the greater light output per Mev. for anthracene than for phenylcyclohexane. Thus, it is reasonable to assume that $n_2 E_o$ is enough greater than $n_1 \cdot \Delta E$ to neglect the first term in the square root.

Again using the approximate relation:

$$\frac{\Delta E}{t} = \frac{dE}{dx} = K\left(\frac{m}{Eo}\right)^{0.76}$$

One then has: $\sigma_m = m\sqrt{\frac{1.69}{n_1 Kt}\left(\frac{Eo}{m}\right)^{0.76}} = \frac{1.69}{n_1 Kt} \cdot m^{0.62} \cdot E_o^{0.38}$

Therefore, in terms of the width of the proton distribution, the width for any other mass particle is:

$$\sigma_m = \sigma_p \cdot \left(\frac{m}{mp}\right)^{0.62} \cdot \left(\frac{Eo}{Eop}\right)^{0.38}$$

C. Energy Correction for the Mass Curves

Let us assume that the low values observed for the proton and deuteron masses are due to saturation of the energy counter as the particle nears the end of its range. For the energy region in which the mass distribution was measured, it was found that 8 Mev must be added to bring the mass 0.89 curve to mass 1.00 and that 16 Mev was necessary to bring the mass 1.58 curve to mass 2.00. Let us calculate here the ratio of the energy correction for protons to that for deuterons on the basis of this assumption, and also obtain a rough measure of the specific ionization at which such saturation occurs in phenylcyclohexane.

Make the simplifying assumption that saturation of the counter occurs suddenly at a specific ionization value, $(dE/dx)_s$. For a particle of mass m this occurs at an energy:

$$E_s = m \frac{KZ^2}{(dE/dx)_s} \cdot \frac{1}{0.76}$$

and at a residual range: $R_s = \dfrac{E_s^{1.76}}{1.76\, KZ^2\, m^{0.76}}$ as shown in Section III.

If the energy of the particle entering the energy counter is E_o, then the measured energy, E_m, is given by:

$$Em = E_o - E_s + \left(\frac{dE}{dx}\right)_s \cdot Rs$$

or: $$(E_o - Em) = E_s - \left(\frac{dE}{dx}\right)_s \cdot Rs$$

Now $(dE/dx)_s$ should be a function of the scintillating material only, and therefore will be the same for all incident particle masses. In particular, for protons and deuterons, we find from the equations above

$$(E_s)_d = 2(E_s)_p \qquad \text{and} \qquad (Rs)_d = 2(Rs)_p$$

Therefore $(E_o - Em)_d = 2(E_o - Em)_p$, in agreement with the observed values.

To calculate the saturation value of specific ionization for this assumption we use the measured value of 8 Mev energy loss for protons and evaluate the above expression.

We find: $(E_o - Em)_p = 8 \text{ Mev.} = (E_s)_p - KZ_p^2 \left(\frac{mp}{Esp}\right)^{0.76} \cdot \frac{E_{sp}^{1.76}}{1.76\, KZ_p^2\, m_p^{0.76}}$

$$= (E_s)_p \left(1 - \frac{1}{1.76}\right)$$

or $(E_s)_p = 18.4 \text{ Mev}$

For this proton, as calculated from the range-energy tables of Aron,[19] the specific ionization in phenylcyclohexane is 29 Mev/gm. cm^{-2}. This is in good agreement with the known saturation values for other scintillators of this type (see Fig. 17).

X. REFERENCES

1. Jackson and Blatt, Rev. Mod. Phys. 22, 77 (1950).
2. Hadley, Kelly, Leith, Segre, Wiegand, and York, Phys. Rev. 75, 351 (1949).
3. Christian and Hart, Phys. Rev. 77, 440 (1951).
4. Chamberlain, Segre, Wiegand, Phys. Rev. 83, 923 (1951).
5. Christian and Noyes, Phys. Rev. 79, 85 (1950).
6. Jastrow, Phys. Rev. 81, 165 and 636 (1951).
7. Levy, Phys. Rev. 88, 725 (1952).
8. Case and Pais, Phys. Rev. 80, 203, (1950).
9. Hildebrand, Phys. Rev. 89, 1090 (1953).
10. Stern, UCRL 1440, (1951) Thesis; also UCRL 2236.
11. Bloom, UCRL 1442, (1951) Thesis; also UCRL 2237.
12. Powell, UCRL 627, (1950).
13. Clark, UCRL 2255, (1953) Thesis.
14. Chew I, Phys. Rev. 74, 809 (1948).
15. Chew II, Phys. Rev. 80, 196 (1950).
16. Chew III, Phys. Rev. 84, 710 (1951).
17. Serber, Phys. Rev. 72, 1008 (1947).
18. York, UCRL 359, (1949) Thesis.
19. Aron, UCRL 121, revised, (1949).
20. Eyges, Phys. Rev. 74, 1534 (1948).
21. Taylor, Jeutschke, Remley, Eby, and Kruger, Phys. Rev. 84, 1034 (1951).
22. Horie, Tamura, Yoshida, Prog. Theor. Phys. 8, 341 (1952).
23. Hadley, UCRL 1542 (1951) Thesis.
24. Communications of Leiden, 1913.
25. Kerr, AECD-3211 (1951).
26. Kirschbaum, UCRL 1967 (1952) Thesis.
27. W. Crandall, private communication.

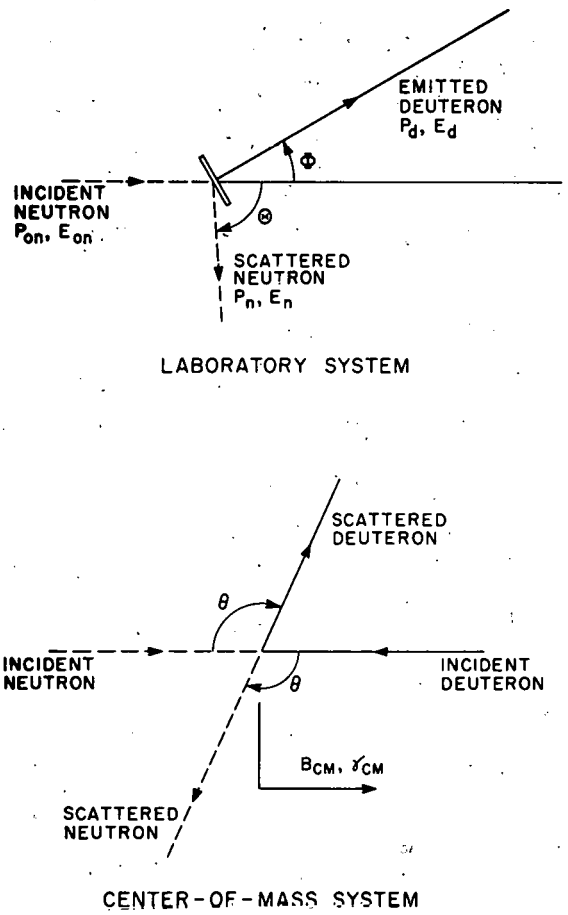

Fig. 1—Kinematics for the elastic scattering of neutrons by deuterons.

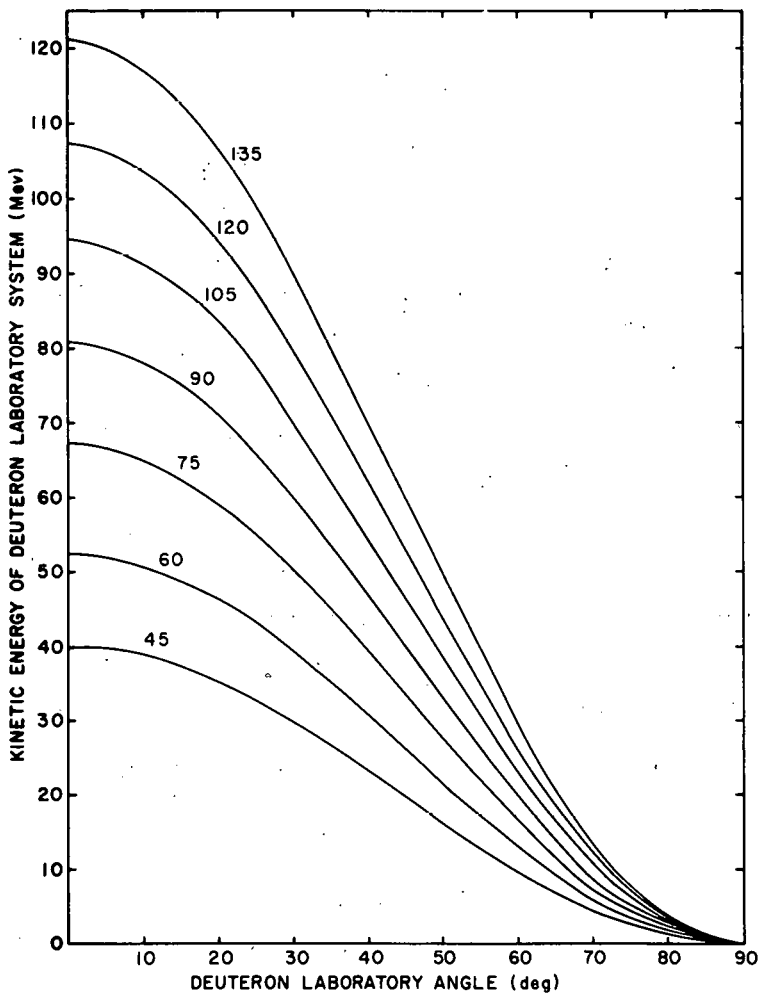

Fig. 2—Plot of kinetic energy of the deuteron vs. its angle of emission in the laboratory system with neutron kinetic energy as a parameter.

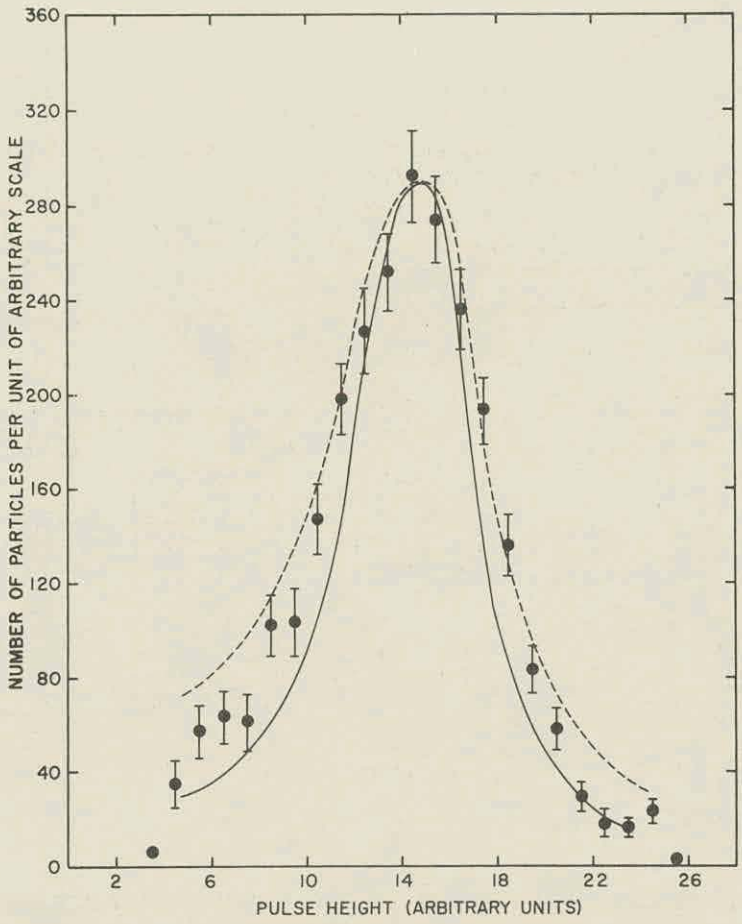

Fig. 3—Spectrum of the 90-Mev neutron beam as measured in the present experiment. The solid curve is for the opaque nucleus and the dotted curve is for the transparent nucleus theory of stripping given by Serber. Variation of the n-p scattering cross section with energy has been included in plotting the curves.

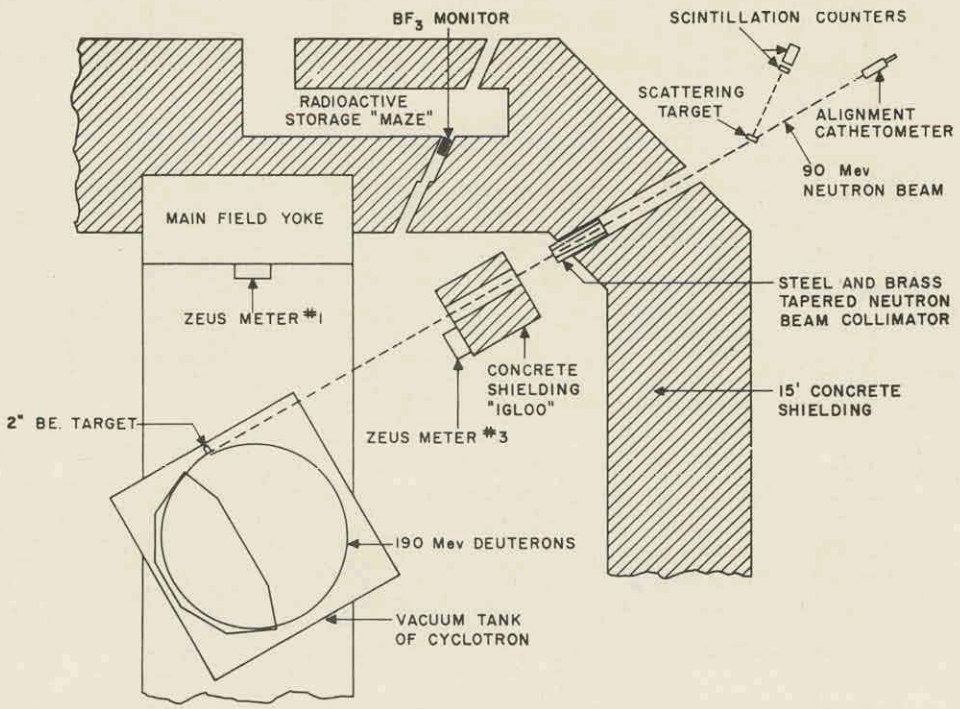

Fig. 4—Plan view of the cyclotron and experimental arrangement.

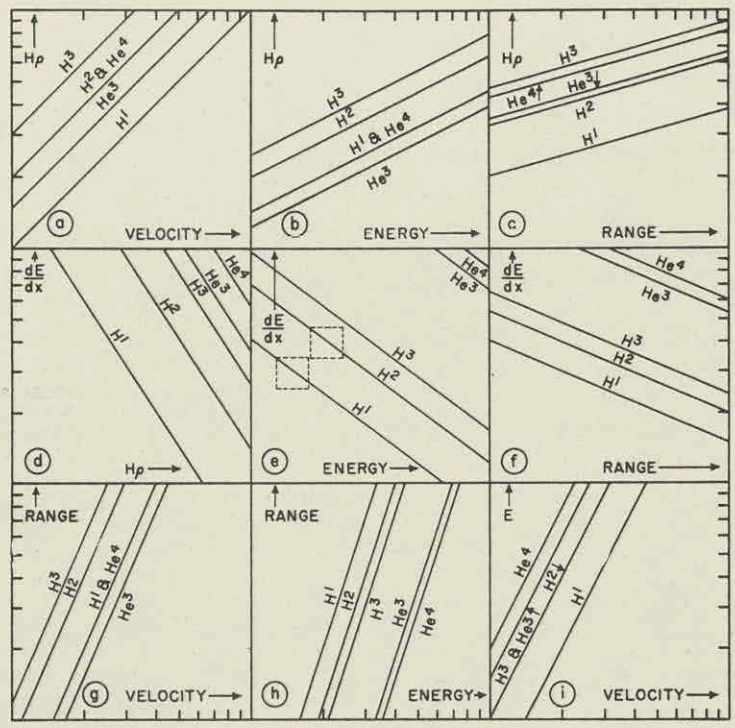

(a) $H\rho \propto \left(\frac{M}{Z}\right) v$

(b) $E \propto \left(\frac{Z^2}{M}\right) (H\rho)^2$

(c) $R \propto \frac{Z^{1.52}}{M^{2.52}} (H\rho)^{3.52}$

(d) $(H\rho) \left(\frac{dE}{dx}\right)^{1.52} \propto Z^{0.48} M^{1.52}$

(e) $\left(\frac{dE}{dx}\right) E^{0.76} \propto M^{0.76} Z^2$

(f) $R \left(\frac{dE}{dx}\right)^{2.32} \propto M Z^{2.64}$

(g) $R \propto \frac{M}{Z^2} v^{3.52}$

(h) $R \propto \frac{E^{1.76}}{Z^2 M^{0.76}}$

(i) $E \propto M v^2$

Fig. 5—Comparison of various experimental methods for particle identification.

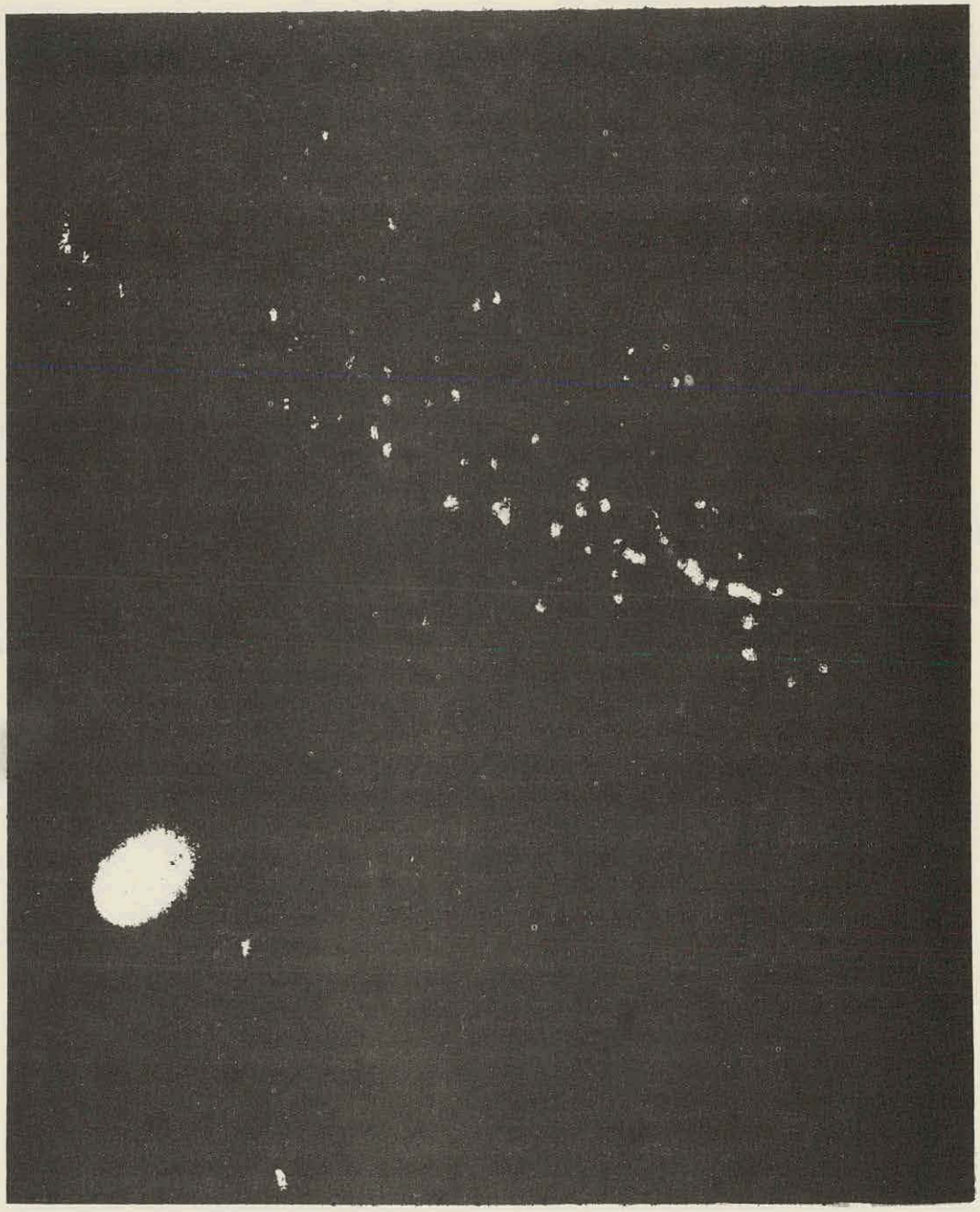

Fig. 6a—Enlargement of a data photograph.

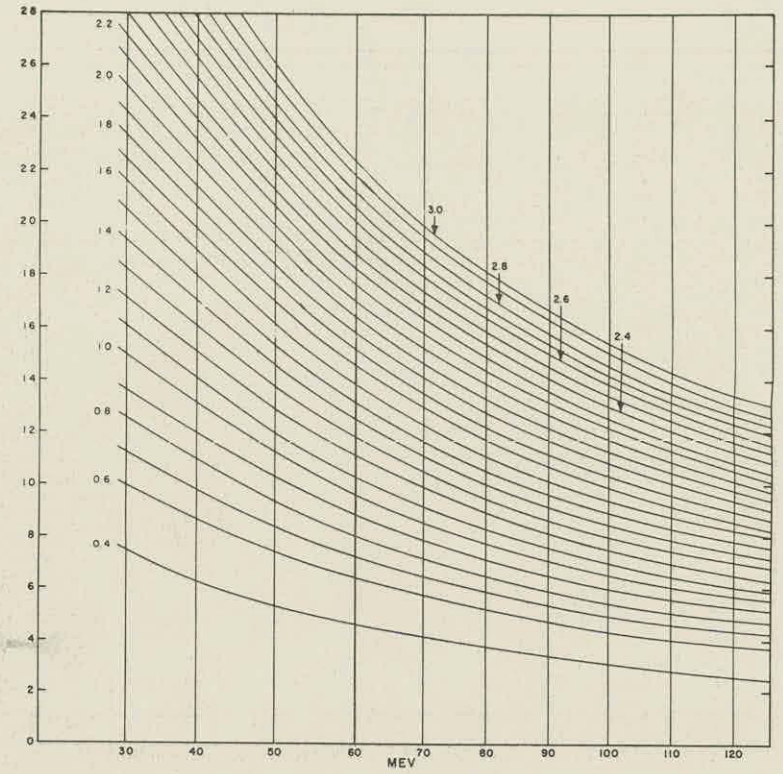

Fig. 6b—Comparison with the calculated iso-mass curves.

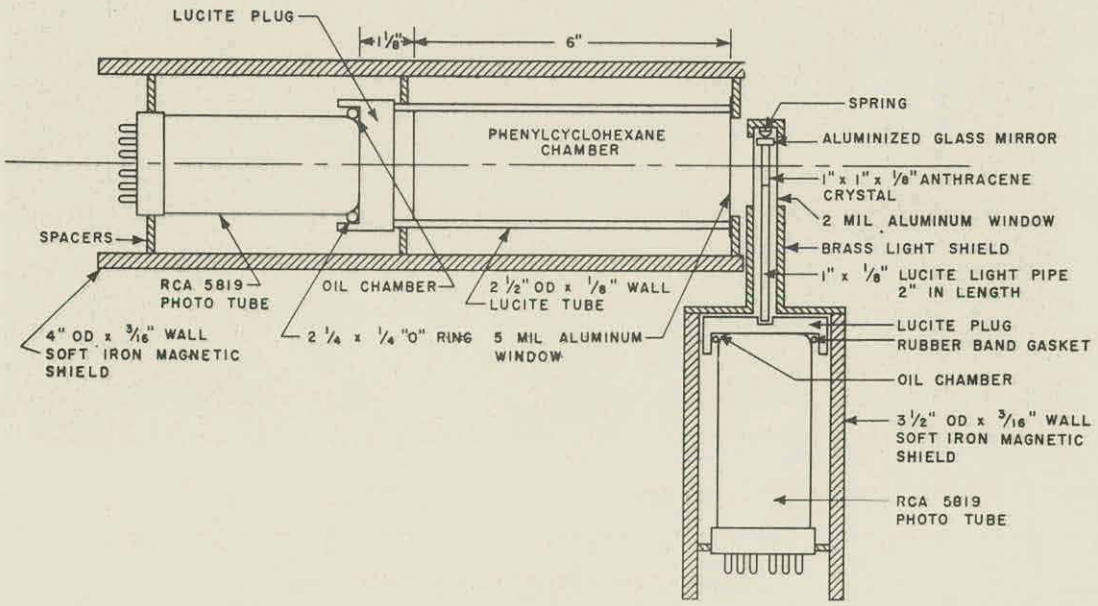

Fig. 7—Detail of the counter construction.

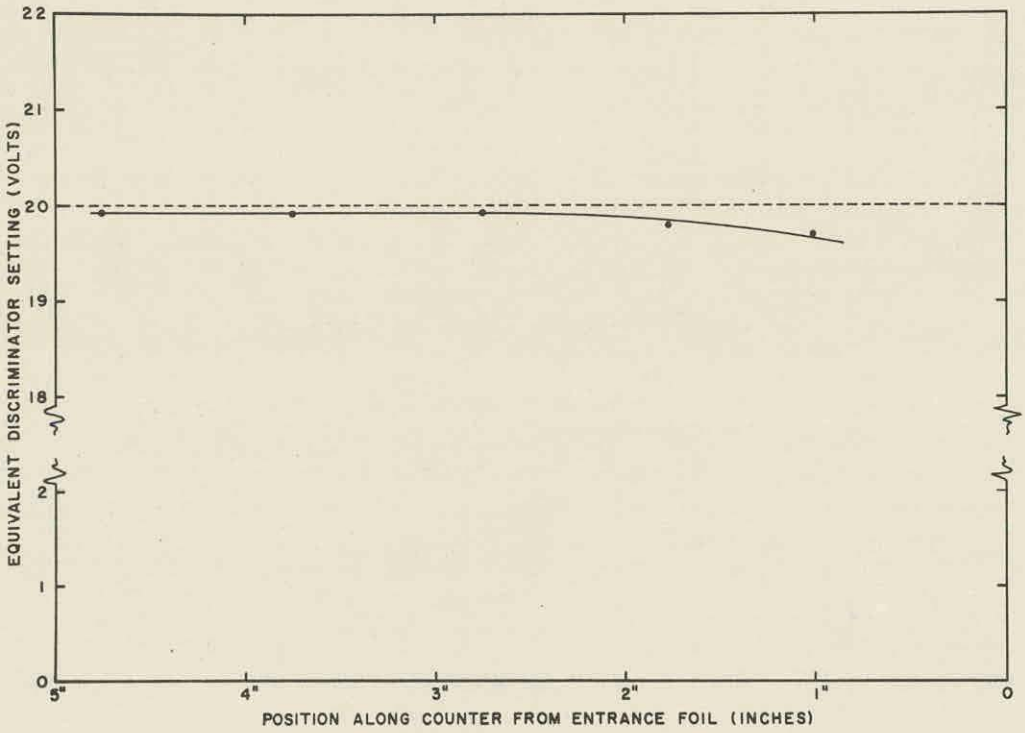

Fig. 8—Pulse-height uniformity of the energy counter.

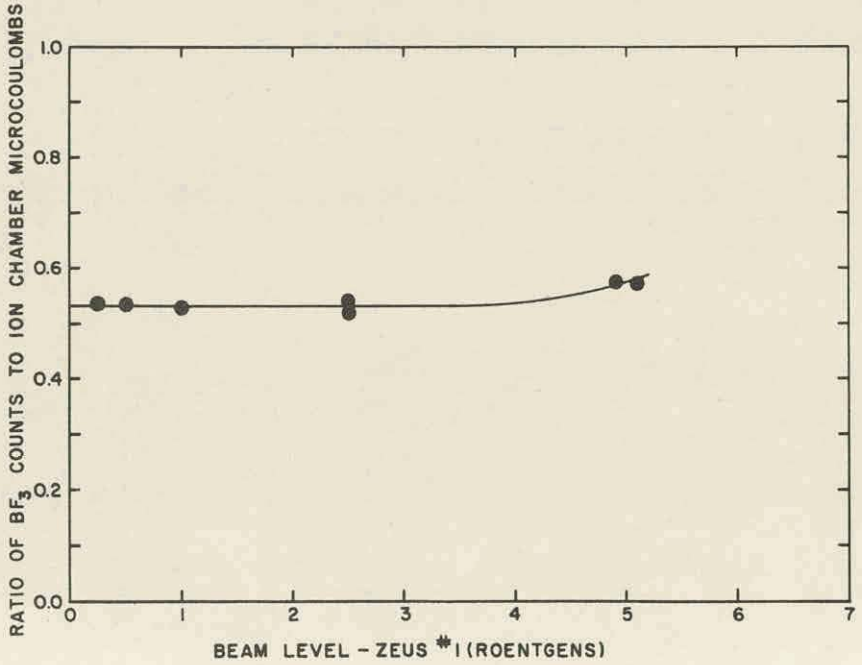

Fig. 9—Response of the BF_3 monitor to changes in beam intensity.

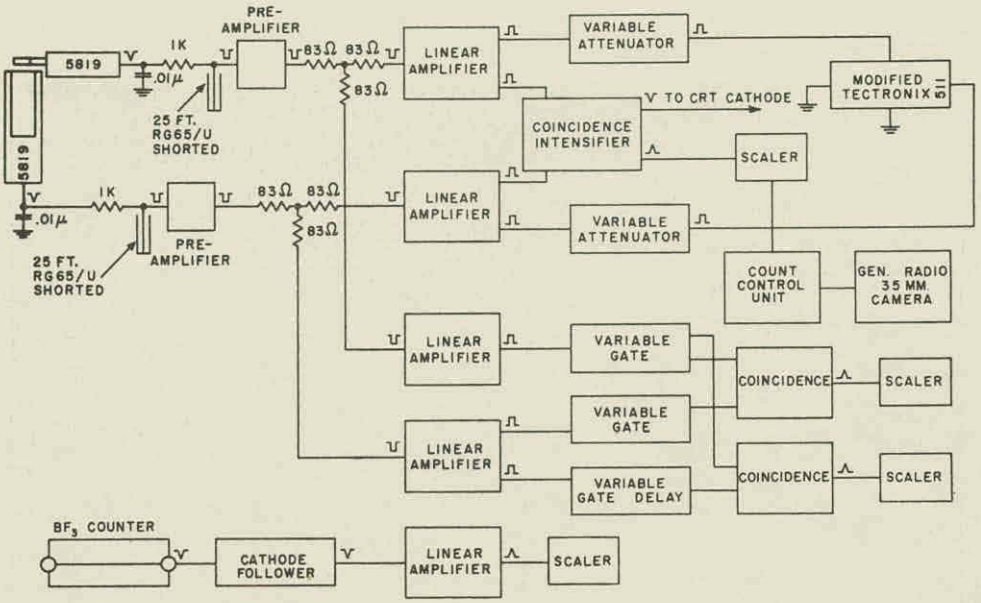

Fig. 10—Block diagram of the electronic circuit.

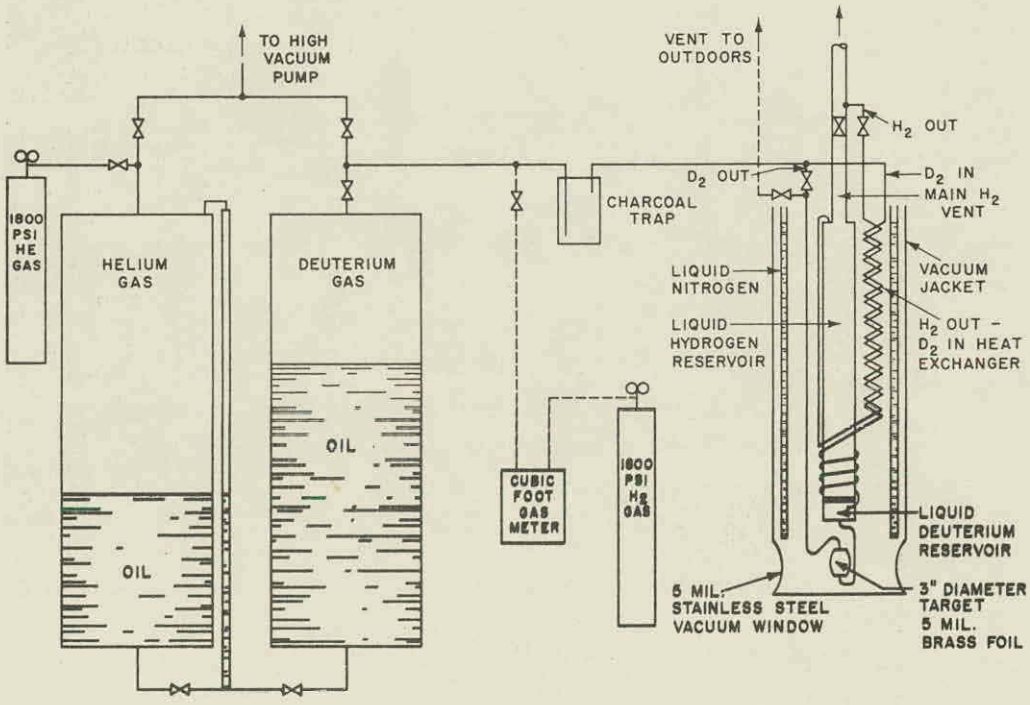

Fig. 11—Schematic of the liquid deuterium condenser system.

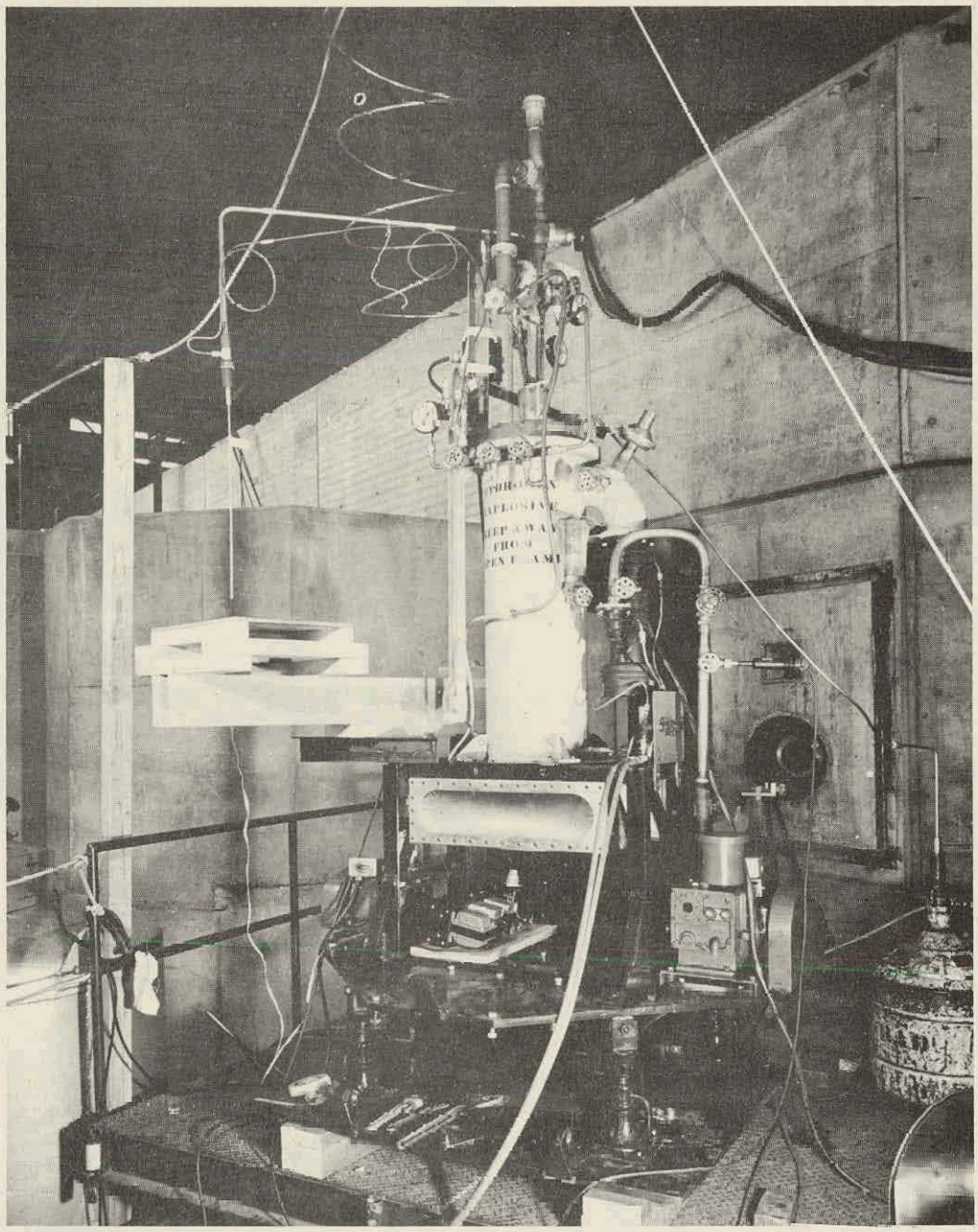

Fig. 12—Photograph of the liquid deuterium system.

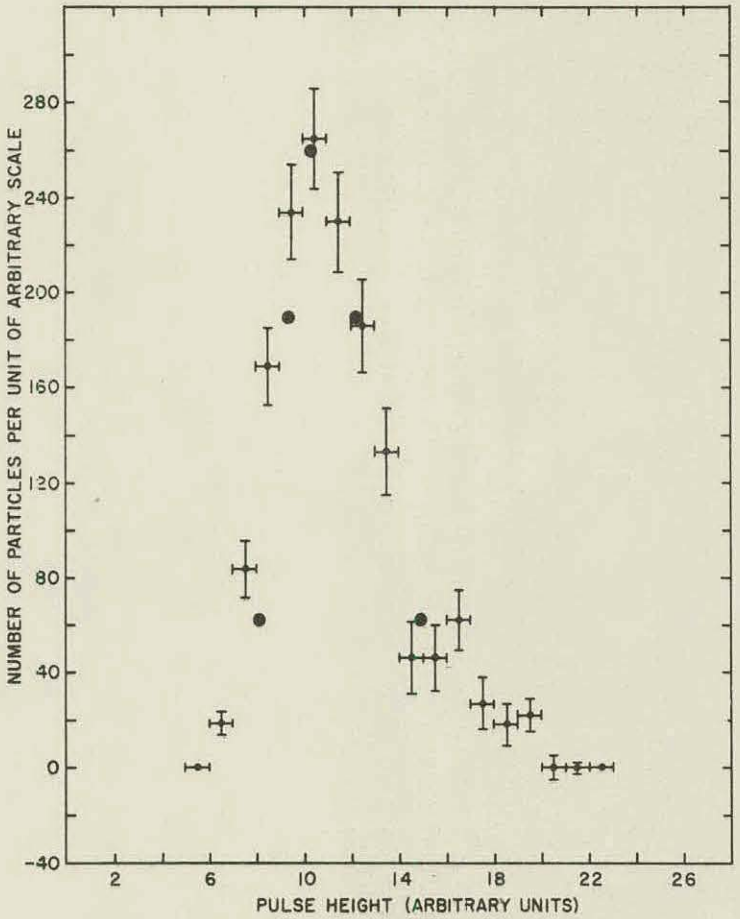

Fig. 13—Distribution in dE/dx for protons scattered at 25° to the beam, obtained from a CH_2-C difference. Solid dots are from the Serber stripping theory.

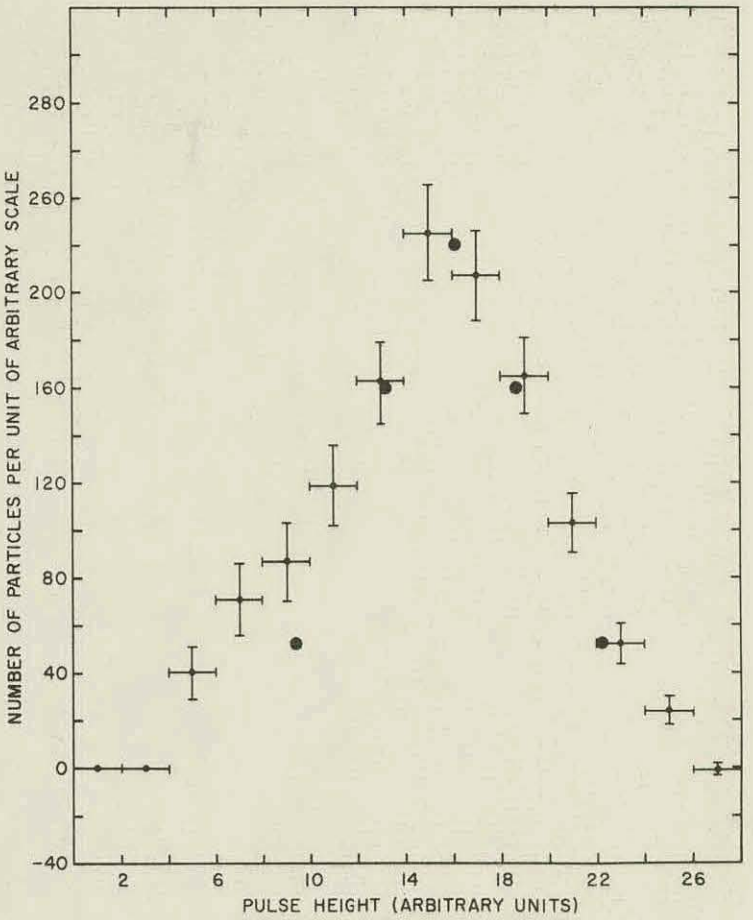

Fig. 14—Distribution in E for protons scattered at 25° to the beam, obtained from a CH_2-C difference. Solid dots are from the Serber stripping theory.

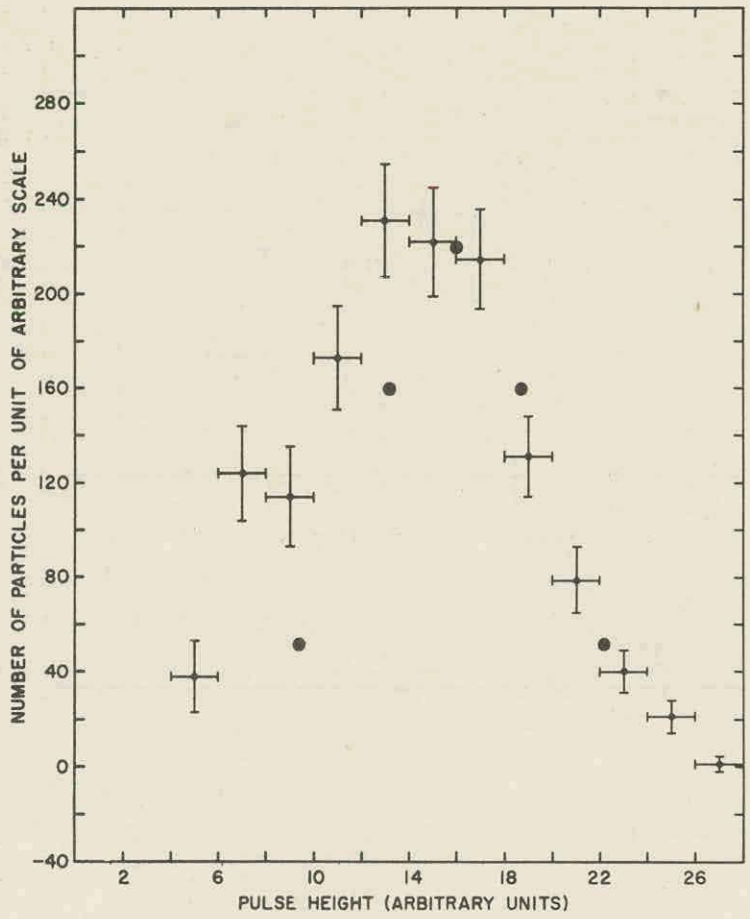

Fig. 15—Distribution in E for protons scattered at 25° to the beam, obtained from a CD_2-C difference. Solid dots are those of Fig. 14 for comparison to the free n-p scattering.

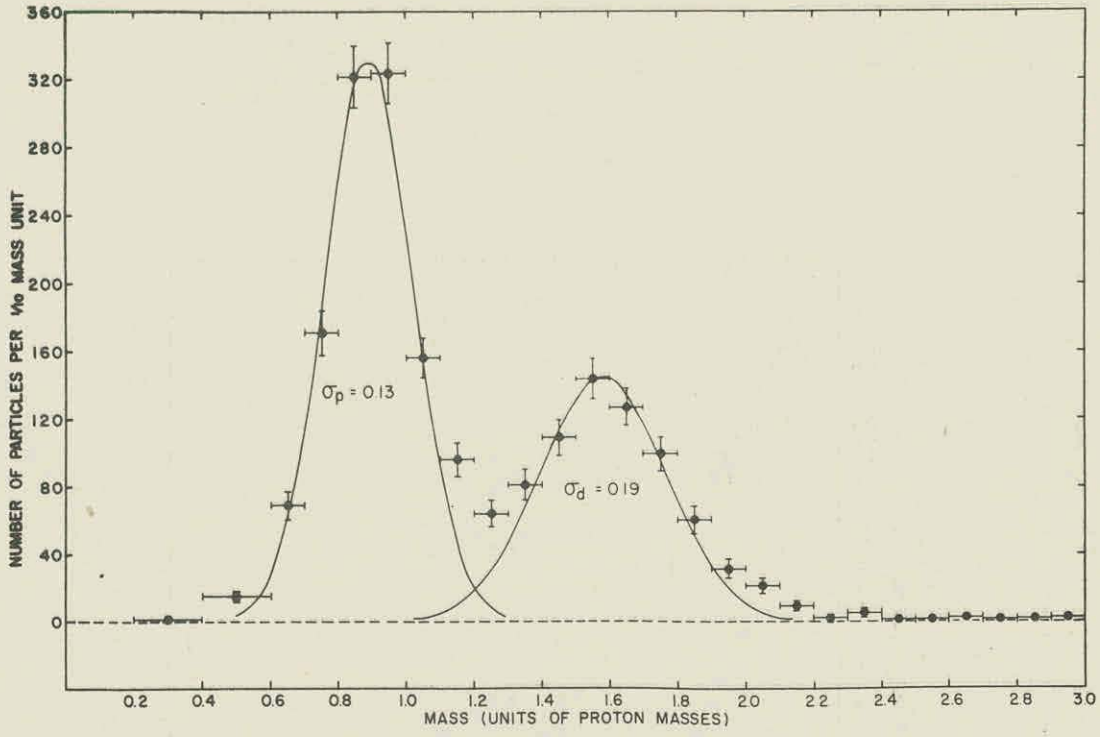

Fig. 16—Distribution in mass for all particles knocked out of carbon at 10° to the neutron beam.

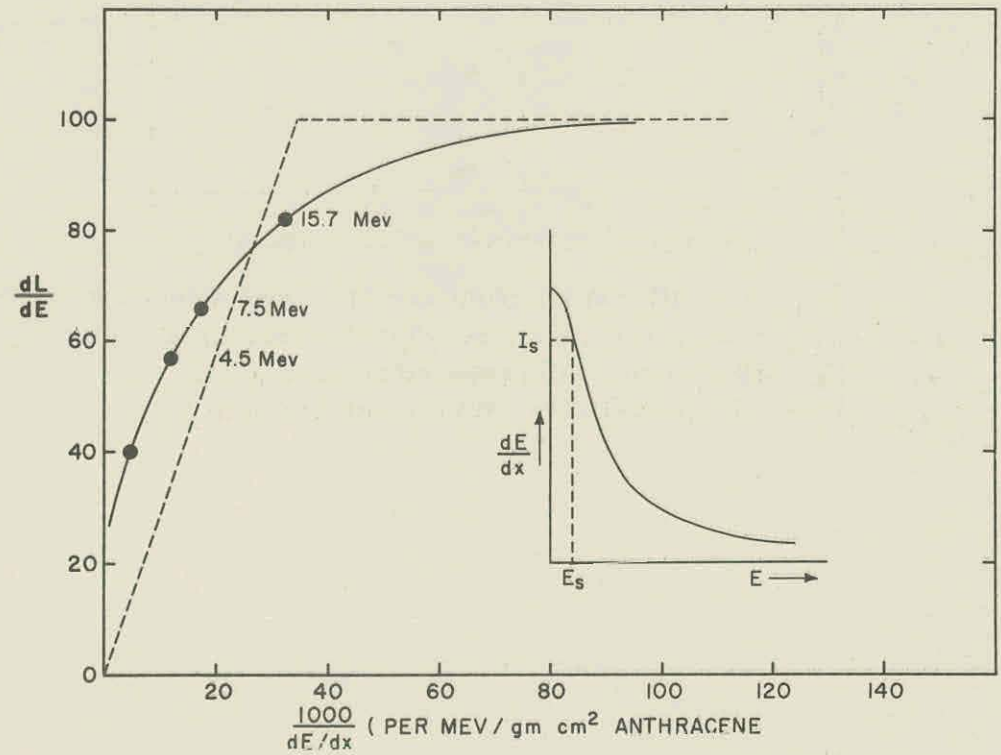

Fig. 17—Curve showing the effect of scintillator saturation near the end of the range for protons in the energy counter.

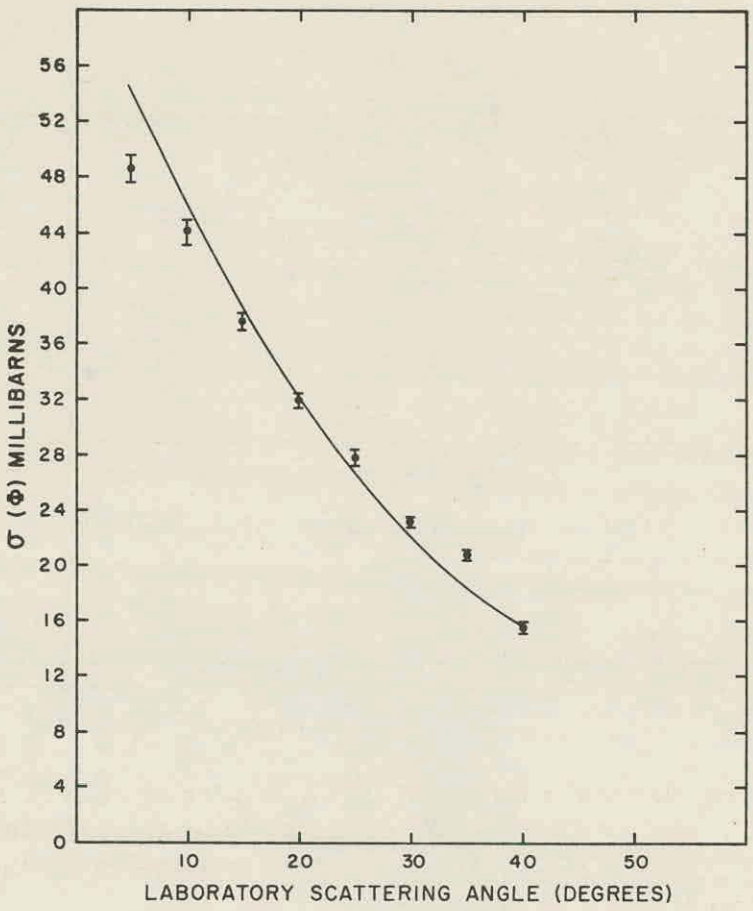

Fig. 18—Differential cross section for neutron-proton scattering as measured by the method of this experiment. Data were normalized to the best curve through the values of Hadley et al.[2]

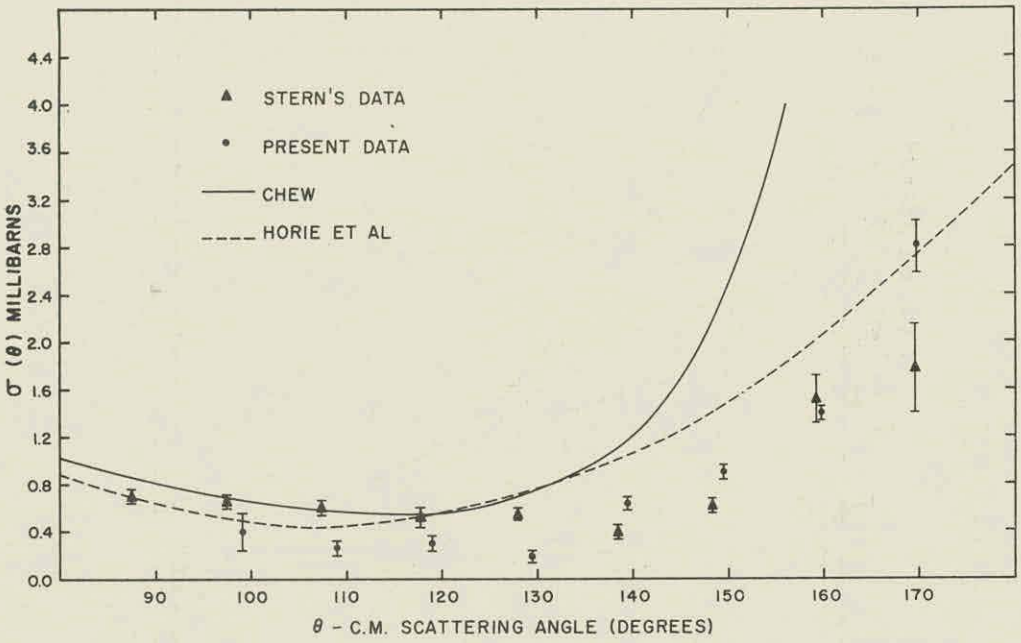

Fig. 19—Experimental results for elastic scattering of 90-Mev neutrons by deuterons. For comparison the results of Stern for 190-Mev deuteron-proton scattering are shown along with the theoretical curves of Chew and of Horie, Tamura, and Yoshida.

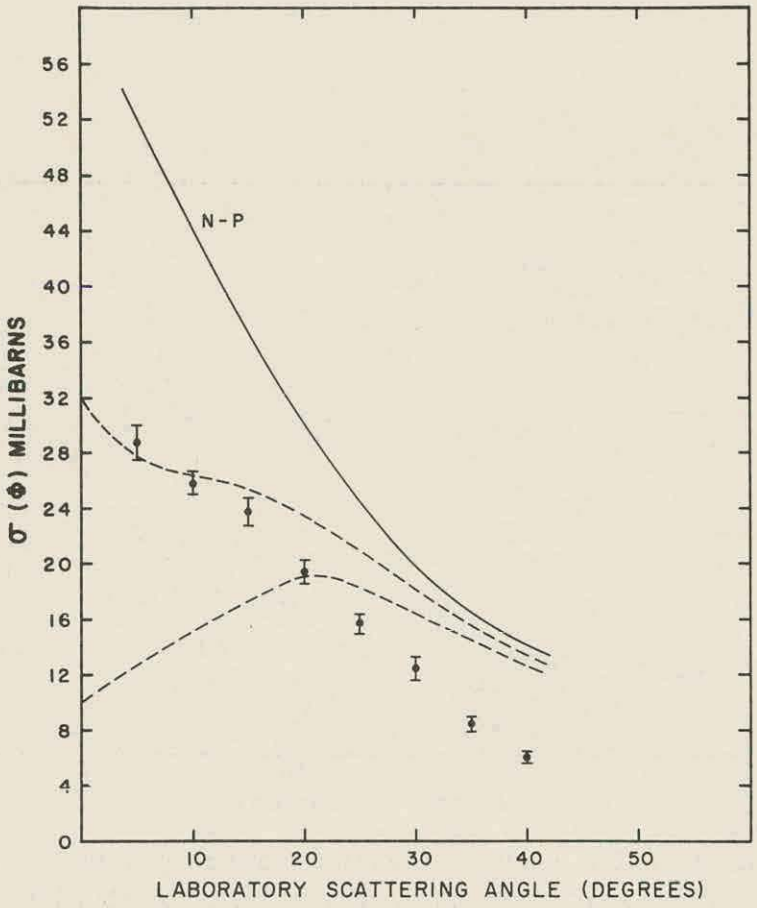

Fig. 20—Experimental results for inelastic scattering of 90-Mev neutrons by deuterons. The solid curve represents the data of Hadley et al.[2] for neutron-proton scattering, and the dotted curves are the theoretical predictions of Chew.